Research Square

Preprints are preliminary reports that have not undergone peer review.
They should not be considered conclusive, used to inform clinical practice,
or referenced by the media as validated information.

Safe-by-design algal EPS based ZnO/zeolite bio-nanocomposite for the removal of BPA

Bikramjit Bhattacharya
Vellore Institute of Technology
Akshada Nair
Vellore Institute of Technology
Abisha Christy Christudoss
Vellore Institute of Technology
Kushal Mukherjee
Vellore Institute of Technology
Krishna Rao Eswar Neerugatti
Vellore Institute of Technology
Amitava Mukherjee
amitav@vit.ac.in

Vellore Institute of Technology

Research Article

Keywords: Bisphenol-A (BPA), Extracellular polymeric substances (EPS), Zinc oxide (ZnO), Zeolite, Photocatalytic degradation

Posted Date: September 12th, 2026

DOI: https://doi.org/10.21203/rs.3.rs-10830446/v1

License: This work is licensed under a Creative Commons Attribution 4.0 International License.
Read Full License

Additional Declarations: No competing interests reported.

Abstract

The existence of endocrine disrupting chemical (EDCs), like bisphenol-A (BPA) creates a huge challenge for conventional wastewater treatment plants. The current study has aimed to develop a hybrid adsorption-photocatalytic material for efficient BPA removal under UV-A irradiation. The characterization of the bio-nanocomposite was using FE-SEM, EDX, FTIR and total organic carbon (TOC). Batch experiments were performed to evaluate the effects of concentration, catalyst dosage, pH and an optimal bio-nanocomposite was developed. The optimized Zeolite:ZnO:EPS ratio of 1:1:0.5 achieved the highest BPA removal under UV-A irradiation. Reactive oxygen species (ROS) scavenging experiments identified superoxide radicals as the dominant oxidative species. In addition, degradation kinetics were determined to be pseudo-first-order. The TOC analysis further confirmed approximately 96% mineralization of BPA after UV-A irradiation. For the biosafety assessments, *Scenedesmus obliquus* and *Allium sativum* were used as model organisms. The results indicate that the presence of EPS reduced oxidative stress and have improved biological compatibility.

1. INTRODUCTION

The release of emerging contaminants (ECs) into aquatic and terrestrial ecosystems poses a serious environmental challenge. The spectrum of ECs is broad and includes pharmaceuticals, personal care products, endocrine disrupting chemicals (EDCs), per- and polyfluoroalkyl substances (PFAS) and microplastics (MPs). Exposure to these ECs has detrimental effects on all life forms (1). Among the known and studied ECs, endocrine disruptors or EDCs such as bisphenol-A (BPA) are being studied due to their persistence and widespread occurrence. Their ability to disrupt growth and hormonal regulation in both humans and animals makes it even more relevant (2). Bisphenol-A (BPA) is a white crystalline powder that is predominantly used to synthesize epoxy resins, polymer materials, and polycarbonate plastic. It also plays an important role in endocrine disruption in human beings (3, 4). The synthesized materials that are improperly disposed of are left within the ecosystem, starting to weather and degrade. The leaching of these plastic materials releases BPA into the environment. With the increasing demand for plastic and plastic products, the chances of exposure to BPA for all life forms become inevitable (5, 6).

Among the several treatment options available for the control of BPA, adsorption remains one of the most studied techniques. Most of the common and known adsorbents show poor regenerative capacity and produce secondary waste (7). This makes the sustainability of these adsorbents an issue when considering the long term. In the context of wastewater treatment plants (WWTPs), along with a proper adsorbent with high regenerative capacity, a catalyst is introduced to create a system for the remediation of the contaminants. Most modern WWTPs involve advanced oxidation processes (AOPs), alone or in combination with an adsorbent system against such contaminants (8). For BPA, multiple studies show the use of hybrid systems for photocatalysis, where graphene oxide (GO) nanoparticles, clay and zeolite have been used successfully. These hybrid setups have shown better adsorption, and advanced oxidation processes (AOPs) help with the degradation of the said pollutant (9, 10).

Among the various advanced oxidation processes for the removal of EDCs, semiconductor-based nano-bioremediation has emerged as one of the most promising solutions. This semiconductor-based approach successfully integrates the high catalytic efficiency of the nanomaterials and combines them with environmentally safe, biologically derived chemicals. Incorporation of naturally occurring porous polymers as support for the photocatalysts has increased their stability, adsorption potential and degradation efficiencies. In addition, it has also shown a reduction in the production of secondary products, which are usually associated with others (1). ZnO also has high quantum yield, excellent photosensitivity, cost-effective fabrication and reduced environmental toxicity (1, 11). Its wide band-gap (3.2–3.37 eV) enables efficient excitation of the electrons under UV light, and helps them generate electron-hole (e /h^+) pairs which can react with the dissolved oxygen and water to produce reactive oxygen species (ROS). Further, ZnO was also able to show better degradation efficiencies in comparison to other widely used catalysts like TiO_2, under UV light conditions (12).

Despite these advantages, pristine ZnO suffers from several intrinsic limitations that reduce its efficiency for photocatalysis under real-life conditions. The rapid recombination of the photogenerated e^-/h^+ pairs, agglomeration of nanoparticles, and difficulty of recovery remain among the top challenges for pristine ZnO (13). In addition, incomplete degradation of BPA yields intermediates like phenol, which is more toxic (14). To improve the dispersion of ZnO and minimize agglomeration, a structural support like zeolite can be added (15, 16). This increases the efficiency of the use of the catalyst, and thereby promotes ROS-mediated degradation along with photocatalysis (17, 18). To further strengthen this binding and the synthesis of sustainable photocatalytic composites, extracellular polymeric substances (EPS) are being considered. The functional groups of EPS facilitate nanoparticle immobilization, improve interfacial interactions, and provide additional adsorption sites for organic pollutants. EPS can reduce nanoparticle aggregation, enhance structural integrity, and improve the reusability of composite materials (19). In addition, EPS can also act as a protective corona, and this coating around ZnO can lower the overall toxicity of the composite (20). Thus, this study aims to integrate ZnO onto a zeolite matrix. This matrix can be further reinforced with algal EPS to develop a bio-nanocomposite. While the role of zeolite would be to improve ZnO dispersion and structural stability, EPS can help in nanoparticle immobilization, pollutant adsorption, and composite integrity. Following physicochemical characterization, the BPA degradation efficiency of the bio-nanocomposite under UV irradiation will be evaluated. Furthermore, the toxicity of the resulting degradation byproducts will be assessed using two biological models to investigate ROS generation and cell viability.

2. METHODOLOGY

2.1 Extraction of Algal EPS

Marine microalgae *Chlorella sp*. were cultured in sterile, membrane filtered natural seawater (NSW) and incubated for 20 days. The algal biomass was harvested during their exponential growth phase (lag phase) using centrifugation at 7000 rpm for 10 minutes at 4°C. The pellets were resuspended in heat

sterilized artificial seawater (ASW; pH 7.8; Table S1), and the resulting suspension was exposed to continuous illumination (3000 lux) using Philips TL-D Super 80 fluorescent lamps (India) for 24 hours. Following the incubation, the culture was centrifuged (Eppendorf, Germany; 5430R) at 13,000 rpm for 15 minutes at 4°C and the supernatant containing the loosely bound EPS (LB-EPS) was separated. The pellets were resuspended in 0.1 M phosphate buffer (pH 7.2) and were treated in a water bath at 70°C for 20 minutes to extract the tightly bound EPS (TB-EPS). The suspension was subjected to centrifugation at 13,000 rpm for 15 minutes at 4°C and filtered through a 0.1 µm syringe filter, followed by 48-hour freeze drying to obtain a white, amorphous powder of EPS (21, 22).

2.2 Synthesis of Bio-nanocomposite

Zeolite (Sigma Aldrich; CAS:1318-02-1) was activated by heating at 150°C in a muffle furnace, followed by treatment with dilute hydrochloric acid (0.1 mM) to enhance surface activity (23). The treated zeolite was then dried in a hot-air oven at 70°C for 6 h. For the preparation of Zeolite:ZnO:EPS bio-nanocomposite, commercially obtained ZnO powder (Sigma Aldrich; CAS:544906-50G) was used without further modification. The composite was prepared at a 1:1:0.5 ratio, with zeolite, ZnO and EPS, respectively, in Milli-Q water. All components were thoroughly mixed and stirred overnight at room temperature (500 rpm) to ensure uniform dispersion and effective interaction among the materials. The resulting suspension was centrifuged at 6500 rpm for 20 min, and the pellets were washed sequentially with ethanol and Milli-Q water to remove unbound particles and impurities. The pellet was dried at 70°C for 6 h in a hot-air oven to yield the zeolite:ZnO:EPS bio-nanocomposite powder, which was subsequently used for characterization and photocatalytic degradation studies, as shown in Fig. 1.

2.3 Characterization

Fourier-transform infrared spectroscopy (FT-IR; IR-Spirit, Shimadzu, Japan) was used to identify the functional groups present on the surfaces of bisphenol A (BPA), the bio-nanocomposite (Zeolite:ZnO:EPS), zeolite, zinc oxide (ZnO), and LB + TB EPS. The surface morphology and elemental composition were examined by field emission scanning electron microscopy (FE-SEM) coupled with energy-dispersive X-ray spectroscopy (EDX) (Carl Zeiss, USA; FEI Quanta FEG 250). The extent of BPA mineralization was determined using a total organic carbon (TOC) analyzer (Shimadzu, Japan).

2.4 Photocatalysis and Degradation

A 1000 mg/L BPA stock was prepared in acetone and diluted with Milli-Q water to obtain the working solution. For the batch photocatalytic studies, the bio-nanocomposites were taken in the ratio of 1:1:0.5, and concentrations of 20, 30, and 40 mg/L were prepared using the BPA solution. The effect of pH was evaluated over the range of 6–10, and adjustment was done using 0.1 M HCl and NaOH. Time optimization was done over regular intervals from 0 to 90 minutes. The initial 30 minutes were allowed to equilibrate the adsorption-desorption optima, and then exposed to UV-A (365 nm) light at room temperature (26°C) in a closed multi-lamp photoreactor equipped with 10 W UV lamps. Degradation of BPA was monitored at 265 nm using a UV-Visible spectrophotometer (UV-2600, Shimadzu, Japan). The

BPA removal efficiency of the bio-nanocomposite was calculated using the following equation, where R% denotes the removal efficiency, C_0 is the initial BPA concentration, and C is the final BPA concentration (23):

$$\varvec{R}\varvec{\%} = \left[1 - \frac{\varvec{C}}{\varvec{C}_0}\right] \varvec{X}\ 100$$

2.5 Biosafety Assessment

2.5.1 Evaluation of cell viability

Healthy *Chlorella* sp. cells from the exponential growth phase were centrifuged and resuspended in autoclaved lake water. The optical density of the culture was adjusted to 0.5. The cell suspension was then incubated for 72 hours with the test samples. After incubation, viable cells were counted using a haemocytometer under an optical microscope. The large and intact cells were considered viable, and the clustered or visibly damaged cells were considered non-viable. The results were expressed with respect to the untreated control.

Allium sativum bulbs were germinated in Hoagland nutrient solution (Table S2) until the roots reached 4–5 cm in length. The germinated cloves were then exposed to the test samples for 4 h. After incubation, the root tips measuring 1–2 cm were cut and stained with 0.25% (w/v) Evans blue for 15 min. The incubated roots were then washed with distilled water for 30 minutes. The roots were then transferred to N, N-dimethylformamide (DMF) and incubated in the dark for 1 hour to extract the dye. The absorbance of the extracted dye was measured at 600 nm using a UV-Vis spectrophotometer (UV-2600, Shimadzu, Japan). The cell death was calculated relative to the control. Cell viability was obtained by subtracting cell death from 100 (24).

2.5.2 Assessment of Reactive Oxygen Species (ROS)

5 mL of *Chlorella* sp. culture was incubated in the dark with 50 µL of 100 mM DCFH-DA (cell-permeable non-fluorescent dye). The culture was incubated for 30 minutes after 72 hours of exposure to the dye. The fluorescence intensity was then measured using a spectrofluorometer (Cary Eclipse fluorescence spectrophotometer, Model – G9800A, Agilent Technologies, USA) at excitation and emission wavelengths of 485 nm and 530 nm, respectively. The ROS production was expressed relative to the untreated control. For *Allium sativum*, 10 roots from each treatment were homogenized in a chilled mortar and pestle using 1x PBS after 4 hours of exposure. The homogenate was then centrifuged at 10,000 rpm for 10 minutes. The supernatant was incubated with 2',7'-dichlorofluorescein diacetate (DCFH-DA; 100 mol/L). After incubation in the dark for 30 minutes, the fluorescence was measured on a fluorescence spectrophotometer with the excitation and emission wavelengths of 485 and 530 nm, respectively. The response of the ROS was compared with the control (24).

3. RESULTS AND DISCUSSION

3.1 Characterization of the Bio-nanocomposite

3.1.1 FE-SEM and EDX Analysis

The FE-SEM micrographs revealed that the zeolite particles were irregularly shaped with rough external surfaces. The external surface contained fine granular deposits, which produced a heterogeneous microstructure with abundant free spaces in between the particles (Fig. 2A). The large polyhedral structures are characteristic of zeolite 13X, and the finer particles adhering to the surface are consistent with the deposition and dispersion of the ZnO nanoparticles (25). Even though localized aggregation of ZnO nanoparticles was observed, the nanoparticles remained widely distributed over the zeolite support. The limited extent of aggregation indicates that the zeolitic framework effectively restricted excessive ZnO agglomeration while maintaining broad nanoparticle dispersion across the support (12). Such an architecture is favourable as it increases the contact area for BPA to be effectively adsorbed while keeping a proximity with the photocatalytic sites. The rough and heterogeneous surface morphology provides additional adsorption domains and helps in mass transfer of BPA towards the catalytic sites. In addition, the uniform dispersion of ZnO would allow better accessibility of the ROS generated under UV irradiation to the adsorbed pollutant (26).

Further, the EDX spectrum (Fig. 2B) confirmed the coexistence of oxygen (O), carbon (C), zinc (Zn), aluminium (Al), silicon (Si), and sodium (Na). Additionally, from the EDX results, the characteristic Zn Kα signal, along with the Si, Al and Na peaks, marks the successful deposition of ZnO on the zeolite matrix (26). Although EPS cannot be directly visualized using FE-SEM, the homogeneous distribution of ZnO observed in the micrographs is consistent with its reported role as a natural stabilizing matrix (27).

3.1.2 FTIR Spectra

The FTIR spectroscopy confirmed the coexistence of the individual components within the bio-nanocomposites (Fig. 3). The spectrum of BPA (Figure S1) exhibits characteristic absorption bands at 3332 cm^{-1}, 2965 cm^{-1}, 1601 and 1506 cm^{-1}, 1222 cm^{-1} and 820 cm^{-1}, corresponding to phenolic O-H stretching, aliphatic C-H stretching, aromatic C = C skeletal vibrations, 1222 cm^{-1} phenolic C-O stretching, and the para-disubstituted aromatic ring of BPA, respectively (28). The zeolite spectrum (Fig. 3A) displayed the characteristic aluminosilicate vibrations at 975 cm^{-1} and 520 cm^{-1} which are characteristic of asymmetric Si-O stretching and Si-O-Si/Si-O-Al bending, respectively. In contrast, the peak for ZnO (Zn-O stretching) has been found below 400 cm^{-1} (Fig. 3B) (29). This preservation of the characteristic vibrations suggests that the process of synthesizing ZnO did not alter the structural integrity of the components. Further, the spectral results are consistent with successful incorporation of ZnO and EPS into the zeolite support (30). The broad adsorption in the hydroxyl region of the FTIR results (Fig. 3C) can be attributed to the overlapping O-H stretching of the surface hydroxyl groups and the polysaccharides and proteins associated with EPS (31). The oxygen-containing functional groups

within EPS are expected to participate in hydrogen bonding and electrostatic interactions with both ZnO nanoparticles and BPA molecules (27). These interactions improve nanoparticle stabilization and also provide additional adsorption sites for the organic contaminants. This stabilization effect of EPS has been linked with the presence of hydroxyl, carboxyl, amino, and polysaccharide functional groups (31, 32). In addition, these functional groups also facilitate the adsorption of the pollutants through hydrogen bonding, π–π interactions, and electrostatic attraction, which helps concentrate the BPA molecules near the ZnO photocatalytic sites (33).

The FTIR results, together with the SEM–EDX observations, therefore support the successful synthesis of the Zeolite:ZnO:EPS bio-nanocomposite. The complementary information obtained from these characterization techniques indicates that the composite possesses the structural features required for efficient adsorption-assisted photocatalytic degradation, namely a stable inorganic support and a functional biopolymeric interface capable of promoting pollutant capture (27, 30, 34).

3.3 The Removal of BPA using the Bio-nanocomposite

3.3.1 Optimization of the Ratio of the Bio-nanocomposite

Different combinations were used to make the bio-nanocomposites, and keeping the experimental conditions intact, the zeolite:ZnO:EPS ratios were varied to estimate the removal efficiency of BPA (Fig. 4D). The three formulations used exhibited distinct adsorption and catalytic behaviours. During the dark adsorption stage, BPA removal increased from approximately 26% for the 1:1:0.1 composite to 31% for the 1:1:1 formulation. This indicates that an increased concentration of EPS enhances the initial adsorption capacity of the material. Following UV-A irradiation, the 1:1:0.5 composite achieved the highest overall BPA removal, whereas the 1:1:1 and 1:1:0.1 formulations reached approximately 81% and 76%, respectively. Thus, it becomes clear that the adsorption capacity cannot be linked directly to their degradation efficiency. Although the 1:1:1 formulation adsorbed more BPA during the dark equilibration stage, its final removal was marginally lower than that of the 1:1:0.5 composite. Thus, efficient photocatalytic degradation depends on achieving an appropriate balance between pollutant adsorption and accessibility of photo-catalytically active sites rather than maximizing adsorption alone (35, 36). Additionally, the lower removal observed for the 1:1:0.1 formulation indicates that insufficient EPS incorporation may reduce the interfacial interactions. Furthermore, in this hybrid system, EPS contributes to making a more homogeneous distribution of the ZnO nanoparticles across the zeolite surface. This increases the probability of pollutant-catalyst contact while minimizing the chances of nanoparticle detachment from the matrix. However, excessive polymers may block the photocatalytic surfaces or alter other metrics. Thus, having an optimum EPS content would help improve the system (37). This is consistent with the findings in this study (Fig. 4D), where the 1:1:0.5 formulation provided the most favourable compromise between adsorption and photocatalytic oxidation.

3.3.2 The Effect of BPA concentration

Figure 4A shows the effect of BPA concentration and its influence on the removal performance of the constructed bio-nanocomposite. The experiments show that the removal efficiency of the bio-nanocomposite gradually decreases with increasing concentrations of BPA. The efficiency was 24% in a solution with BPA at 20 mg/L, which gradually decreased to 9% at 30 mg/L, and to 1% at 40 mg/L solutions. After subjecting the samples to UV-A treatments, the overall removal efficiencies reached to 82%, 76% and 66% at 20, 30 and 40 mg/L of BPA concentration, respectively, showing a decline in photocatalytic potential with an increase in the concentration of BPA. The reduced removal efficiencies at higher concentrations of BPA can be associated with the decreasing catalyst-to-pollutant ratio in the system, resulting in saturation of the active sites of the catalyst. This phenomenon is consistent with the Langmuir-Hinshelwood (L-H) mechanism, which explains how the finite number of active sites can reduce the overall degradation efficiency (35, 38). In addition, the increased BPA concentrations can result in increased absorbance and light attenuation, lower electron-hole generation within the ZnO nanoparticles and reduced production of ROS. Such concentration-dependent decrease in efficiencies has been seen for TiO_2 as well against environmental contaminants (39–41). The highest removal efficiency obtained at 20 mg/L also signifies that lower concentrations created a favourable balance between adsorption and photocatalysis. Further, in the context of wastewater treatment, optimisation of the catalyst to pollutant ratio would be critical.

3.3.3 The Effect of Catalyst Dosage

The effect of catalyst dosage was tested over a range of 500 mg/L up to 2000 mg/L, as shown in Fig. 4B. The BPA removal efficiency was approximately 36%, 24%, and 31% for catalyst loadings of 500, 1000, and 2000 mg/L, respectively, during the dark adsorption phase. These numbers improved post UV-A irradiation treatment, and the removal efficiencies improved to 86%, 82% and 82% from 36%, 24%, and 31%, respectively. Although the adsorption capacities varied with doses, the final effective removal of BPA fell in the narrow region of 82–86%. The highest removal efficiency was obtained at 500 mg/L (86%; Fig. 4B), and no further improvement was seen at concentrations beyond this level. This, therefore, means that the system has reached its operational optimum. For heterogeneous photocatalytic systems, similar behaviour has been reported where loading can influence the availability of active sites. This availability, however, reaches a plateau since photon absorption becomes the rate-limiting step rather than catalyst availability (36, 42). The absence of improvement at the higher concentrations might be due to the increased particle concentration within the suspension. At higher concentrations of loading, the particle-particle interactions may aggregate and increase the scattering of light. This would reduce the effective penetration of the UV rays into the reaction medium, and a fraction of the photocatalyst surface may become insufficiently illuminated and provide a false negative result (43, 44).

3.3.4 The Effect of pH

The effect of pH on the removal efficiency of BPA was tested at pH 6, 8 and 10 (Fig. 4C). During the pre-UV-A irradiation stages, the adsorption rates remained consistent around 31–35%. However, post UV-A exposure, the efficiencies changed to 81%, 81% and 79% at pH 6, 8 and 10, respectively. This low fluctuation across three different pH ranges shows that the bio-nanocomposite remains stable across

the pH range 6–10, and maintains performance both near-neutral and moderately alkaline conditions. This negligible fluctuation in performance also means that the components of the composites may have synergistic contributions. For instance, the aluminosilicate framework of zeolite provides a stable network for adsorbing the aromatic organic molecules, while ZnO creates ROS in the presence of UV-A to oxidise the pollutant. Similarly, the EPS, having its available functional groups, would help in enrichment of the pollutants and improve adsorption (45, 46). Out of the three, at pH 10, a slight reduction in the removal efficiency was observed (79%; Fig. 4C). This could be possible due to the deprotonation of BPA, because its pK_a is 9.6–10.2 (47). However, the observed decrease was minimal, which means that the bio-nanocomposite can successfully compensate for these changes in solution chemistry. Additionally, the broader tolerance could prove to be advantageous in case of wastewater treatment applications.

The optimization studies thus show that the removal of BPA requires a balance of adsorption and photocatalysis. The highest performance of removal was achieved at 1:1:0.5 (zeolite:ZnO:EPS) with a catalyst dosage of 500 mg/L. This also suggests that an excessive loading of EPS or catalysts would hinder the active sites and reduce the penetration of light. In addition, increasing the concentration of BPA reduced the efficiency, which supports the role of an optimal catalyst-to-pollutant ratio and active site availability. Further, the stable performance of the bio-nanocomposite at pH 6–10 shows a good level of tolerance of the bio-nanocomposite.

3.4 Mineralization of BPA

The total organic carbon (TOC) analysis confirmed BPA removal accompanied by mineralization rather than simple parent-compound disappearance. During the initial dark adsorption stage (30 min), TOC removal was only 19%. This indicates that the zeolite-EPS matrix had mainly adsorbed BPA at the surface rather than destroying it. After 90 min of UV-A irradiation, TOC removal increased to 96% (Fig. 5). This shows that there was extensive conversion of BPA and its degradation products into inorganic end products. This sharp increase after irradiation supports an adsorption-assisted photocatalytic mechanism, where the zeolite and EPS enrich BPA near the ZnO surface during the dark phase, and UV-A activation of ZnO generates ROS that can oxidize the adsorbed BPA (48).

3.5 The role of reactive oxygen species in the photocatalytic removal of BPA

The radical scavenging results showed that superoxide-mediated pathways were the main pathways for BPA degradation. Among the scavengers examined, p-benzoquinone most strongly inhibited degradation, indicating that superoxide radicals ($\bullet O_2^-$) were the major reactive species (Fig. 6). Hydroxyl radicals (•OH) and singlet oxygen ($^1O_2$) played a minor role, as isopropanol and sodium azide also decreased the degradation efficiency. Conversely, the smallest effect was found with ammonium oxalate, indicating that the direct hole-mediated oxidation was of relatively minor importance (49).

ZnO is a large band gap semiconductor (3.2–3.37 eV) being activated mainly under UV-A irradiation. Under excitation, ZnO produces electron-hole pairs; the photogenerated electrons reduce dissolved oxygen to generate $\bullet O_2^-$, while the holes can oxidize surface-adsorbed water or hydroxyl groups to generate •OH. These reactive species attack the aromatic structure of BPA and lead to hydroxylation, bond cleavage and ring opening. The zeolite–EPS architecture could aid this process by concentrating BPA near the ZnO surface and reducing nanoparticle aggregation, thereby increasing the accessibility of the reactive sites (50, 51).

The degradation kinetics also supported the photocatalytic degradation of BPA, which was observed. The pseudo-first-order model matched the experimental data better (R^2 = 0.9985) than the pseudo-second-order model (R^2 = 0.9707) (Figure S2). The pseudo-first-order rate constant was found to be 0.02403 min^{-1}, indicating that BPA degradation under the experimental conditions followed mainly pseudo-first-order kinetics.

3.7 Biosafety Assessment and the Protective Role of EPS

The biosafety data show that EPS substantially improved the biological compatibility of the nanocomposite. In both *Scenedesmus obliquus* and *Allium sativum* roots, the EPS containing formulations retained higher cell viability than the corresponding EPS free materials at both 10 and 100 mg/L. In addition, the EPS containing systems also produced lower intracellular ROS (Fig. 8). This shows that the EPS coating has helped reduce oxidative stress and cellular injury. The same protective trend remained evident in the BPA removal experiments. As the treatments progressed, cell viability increased, and the ROS declined (Fig. 7). This shows that biological recovery is followed by contaminant removal. Therefore, together, these patterns show a direct link between bioremediation efficiency and biosafety.

In this system, EPS acts as a biopolymeric shield around the inorganic particles. The polysaccharides, proteins, uronic acids, hydroxyl groups, amino groups, and carboxyl groups interact with the nanoparticle surfaces through coordination, electrostatic interactions, and steric stabilization. This helps reduce aggregation and moderates direct contact with cells. In addition, the EPS layer likely buffers the release of ROS and helps reduce the toxic activity of ZnO. At the same time, the EPS layer likely acts to buffer the release of reactive surface species and to help confine ZnO activity to the pollutant-removal interface rather than the biological environment. Therefore, EPS not only can promote pollutant capture and photocatalyst dispersion but also act as a protective interface to suppress excessive ROS generation and improve biosafety. (23, 51).

4. Conclusion

The current study has successfully developed a bio-nanocomposite which can act as a multifunctional material for the efficient removal of BPA. The bio-nanocomposite, which contains Zeolite, ZnO and EPS, works on the combined principles of adsorption and photocatalytic degradation. Material characterization confirmed the successful incorporation of ZnO and EPS onto the zeolitic support, which

produces a heterogeneous composite. This enables it to enrich BPA at the catalyst surface and promote its subsequent photocatalytic oxidation processes. The ratio of 1:1:0.5 for Zeolite:ZnO:EPS was found to give the optimum balance and thus was selected for the rest of the experiments. The bio-nanocomposite has also shown high levels of activity at pH ranges 6 to 10. Further, the composite at lower catalyst loading has shown better adaptability under variable conditions.

The study of BPA degradation was primarily mediated by superoxide radicals, with hydroxyl radicals playing a secondary role. The degradation was determined to follow pseudo-first-order kinetics. Additionally, the TOC analysis shows that 96% mineralization was achieved following UV-A irradiation. This confirmed that BPA removal proceeded through extensive oxidative degradation rather than simple adsorption or partial transformation. In addition, it can also be concluded that EPS significantly enhances the biological compatibility of the composite. Furthermore, EPS has also shown reduced toxicity of the treated effluents and supports safer degradation of the pollutant by limiting ROS and thereby increasing cell viability. The developed Zeolite:ZnO:EPS bio-nanocomposite, therefore, represents a promising solution for the remediation of BPA. Its combined adsorption and photocatalytic mechanism, with high mineralization efficiency, makes it a good choice in wastewater treatment.

Declarations

Ethics, Consent to Participate, and Consent to Publish declarations

Not applicable

Competing Interests:

The authors declare that they have no competing interests.

Funding:

Not applicable

Author Contribution

Bikramjit Bhattacharya and Akshada Nair: Conceptualization, Investigation, Methodology, Visualization, Formal analysis, Writing-Original Draft. Abisha Christy Christudoss: Methodology, Visualization, Formal analysis. Kushal Mukherjee: Formal Analysis, Writing-Original Draft. Krishna Rao Eswar Neerugatti: Methodology, Writing- Review and editing. Amitava Mukherjee: Conceptualization, Methodology, Formal analysis, Supervision, Writing- Review and editing.

Acknowledgement

The authors would like to acknowledge Vellore Institute of Technology (VIT), Vellore, for providing the facilities used in this study.

Data Availability

The datasets used and/or analyzed during the current study are available from the corresponding author on reasonable request.

References

1. Ahmed SF, Mofijur M, Nuzhat S, Chowdhury AT, Rafa N, Uddin MdA, et al. Recent developments in physical, biological, chemical, and hybrid treatment techniques for removing emerging contaminants from wastewater. J Hazard Mater. 2021;416:125912. doi:10.1016/j.jhazmat.2021.125912
2. Metcalfe CD, Bayen S, Desrosiers M, Muñoz G, Sauvé S, Yargeau V. An introduction to the sources, fate, occurrence and effects of endocrine disrupting chemicals released into the environment. Environ Res. 2022;207:112658. doi:10.1016/j.envres.2021.112658
3. Corrales J, Kristofco LA, Steele WB, Yates BS, Breed CS, Williams ES, et al. Global Assessment of Bisphenol A in the Environment: Review and Analysis of Its Occurrence and Bioaccumulation. Dose-Response. 2015;13(3):1559325815598308. doi:10.1177/1559325815598308
4. Ighalo JO, Kurniawan SB, Khongthaw B, Buhari J, Chauhan PK, Georgin J, et al. Bisphenol A (BPA) toxicity assessment and insights into current remediation strategies. RSC Adv. 2024;14(47):35128–62. doi:10.1039/D4RA05628K
5. Borah SJ, Gupta AK, Gupta A, Bhawna, Kumar S, Sharma R, et al. Grasping the supremacy of microplastic in the environment to understand its implications and eradication: a review. J Mater Sci. 2023;58(32):12899–928. doi:10.1007/s10853-023-08806-8
6. Watt E, Picard M, Maldonado B, Abdelwahab MA, Mielewski DF, Drzal LT, et al. Ocean plastics: environmental implications and potential routes for mitigation – a perspective. RSC Adv. 2021;11(35):21447–62. doi:10.1039/D1RA00353D
7. Mishra A, Goel D, Shankar S. Bisphenol A contamination in aquatic environments: a review of sources, environmental concerns, and microbial remediation. Environ Monit Assess. 2023;195(11):1352. doi:10.1007/s10661-023-11977-1
8. Rout PR, Zhang TC, Bhunia P, Surampalli RY. Treatment technologies for emerging contaminants in wastewater treatment plants: A review. Sci Total Environ. 2021;753:141990. doi:10.1016/j.scitotenv.2020.141990
9. Waleed S, Haroon M, Ullah N, Tuzen M, Rind IK, Sarı A. A comprehensive review on advanced trends in treatment technologies for removal of Bisphenol A from aquatic media. Environ Monit Assess.

2024;197(1):83. doi:10.1007/s10661-024-13460-x

10. El Hankouri F, Charki A, Bahouch M, Ghalit M, Elyoussfi A, El Ouarghi H, et al. Recent advances in adsorption and advanced oxidation processes for industrial wastewater treatment: Toward integrated and sustainable approaches. Mater. 2026;12:102086. doi:10.1016/j.nxmate.2026.102086
11. Dagareh MI, Hafeez HY, Mohammed J, Kafadi ADG, Suleiman AB, Ndikilar CE. Current trends and future perspectives on ZnO-based materials for robust and stable solar fuel (H2) generation. Chem Phys Impact. 2024;9:100774. doi:10.1016/j.chphi.2024.100774
12. Abo R, Kummer NA, Merkel BJ. Optimized photodegradation of Bisphenol A in water using ZnO, TiO_2 and SnO_2 photocatalysts under UV radiation as a decontamination procedure [Internet]. Treatment: Advanced oxidation;2016 [cited 2026 Jul 29]. Available from: https://dwes.copernicus.org/preprints/dwes-2016-5/dwes-2016-5.pdf doi:10.5194/dwes-2016-5
13. Baig A, Siddique M, Panchal S. A Review of Visible-Light-Active Zinc Oxide Photocatalysts for Environmental Application. Catalysts. 2025;15(2):100. doi:10.3390/catal15020100
14. Kolvenbach B, Schlaich N, Raoui Z, Prell J, Zühlke S, Schäffer A, et al. Degradation Pathway of Bisphenol A: Does *ipso* Substitution Apply to Phenols Containing a Quaternary α-Carbon Structure in the *para* Position? Appl Environ Microbiol. 2007;73(15):4776–84. doi:10.1128/AEM.00329-07
15. Al-Jubouri SM, Al-Batty S, Al-Hamd RKhS, Sims R, Hakami MW, Sk MH. Sustainable environment through using porous materials: A review on wastewater treatment. Asia-Pac J Chem Eng. 2023;18(4):e2941. doi:10.1002/apj.2941
16. García H, Roth HD. Generation and Reactions of Organic Radical Cations in Zeolites. Chem Rev. 2002;102(11):3947–4008. doi:10.1021/cr980026x
17. Sacco O, Matarangolo M, Vaiano V, Libralato G, Guida M, Lofrano G, et al. Crystal violet and toxicity removal by adsorption and simultaneous photocatalysis in a continuous flow micro-reactor. Sci Total Environ. 2018;644:430–8. doi:10.1016/j.scitotenv.2018.06.388
18. Zhou P, Wang F, Shen Y, Duan X, Zhao S, Chen X, et al. Removal of Emerging Organic Pollutants by Zeolite Mineral (Clinoptilolite) Composite Photocatalysts in Drinking Water and Watershed Water. Catalysts. 2024;14(4):216. doi:10.3390/catal14040216
19. Flemming HC, Wingender J, Szewzyk U, Steinberg P, Rice SA, Kjelleberg S. Biofilms: an emergent form of bacterial life. Nat Rev Microbiol. 2016;14(9):563–75. doi:10.1038/nrmicro.2016.94
20. Debroy A, Sinha AK, Maity C, Pulimi M, Peijnenburg WJGM, Mukherjee A. In-situ and ex-situ EPS-corona formation on ZnO QDs mitigates their environmental toxicity in the freshwater microalgae Chlorella sp. J Hazard Mater. 2025;486:137034. doi:10.1016/j.jhazmat.2024.137034
21. Debroy A, Pulimi M. Unraveling the interactions between graphene family nanomaterials and algal-EPS: a novel perspective on toxicity mitigation towards marine microalgae. Environ Sci Eur. 2025;37(1):233. doi:10.1186/s12302-025-01268-6
22. Roy N, Roy S, Debroy A, Mukherjee A. Chlorella sp. EPS loaded alginate microsphere: A novel bionanomaterial for adsorptive removal of sulfamethoxazole from the aqueous solutions. Environ Technol Innov. 2024;33:103513. doi:10.1016/j.eti.2023.103513

23. Bhattacharya B, Debroy A, Viswanathan D, Anandraj FN, Neerugatti KE, Mukherjee A. Ecofriendly algal extracellular polymeric substance-based nanobiocomposite for photodegradation of bisphenol A. iScience. 2025;28(12):114021. doi:10.1016/j.isci.2025.114021
24. Bhattacharya B, Debroy A, Viswanathan D, Anandraj FN, Neerugatti KE, Mukherjee A. Ecofriendly algal extracellular polymeric substance-based nanobiocomposite for photodegradation of bisphenol A. iScience. 2025;28(12):114021. doi:10.1016/j.isci.2025.114021
25. David Elena. Evaluation of Behavior of 13X Zeolite Modified with Transition Metals for Catalytic Applications. Perlepes S, editor. Bioinorg Chem Appl. 2022;2022(1):7352074. doi:10.1155/2022/7352074
26. Li M, Wu L, Zhang Z, Mai K. Preparation of ZnO-supported 13X zeolite particles and their antimicrobial mechanism. J Mater Res. 2017;32(22):4232–40. doi:10.1557/jmr.2017.410
27. Flemming HC, Van Hullebusch ED, Little BJ, Neu TR, Nielsen PH, Seviour T, et al. Microbial extracellular polymeric substances in the environment, technology and medicine. Nat Rev Microbiol. 2025;23(2):87–105. doi:10.1038/s41579-024-01098-y
28. Rathnayake SI, Xi Y, Frost RL, Ayoko GA. Environmental applications of inorganic–organic clays for recalcitrant organic pollutants removal: Bisphenol A. J Colloid Interface Sci. 2016;470:183–95. doi:10.1016/j.jcis.2016.02.034
29. Eren S, Türk FN, Arslanoğlu H. Synthesis of zeolite from industrial wastes: a review on characterization and heavy metal and dye removal. Environ Sci Pollut Res. 2024;31(29):41791–823. doi:10.1007/s11356-024-33863-0
30. Alswat AA, Ahmad MB, Saleh TA, Hussein MZB, Ibrahim NA. Effect of zinc oxide amounts on the properties and antibacterial activities of zeolite/zinc oxide nanocomposite. Mater Sci Eng C. 2016;68:505–11. doi:10.1016/j.msec.2016.06.028
31. Flemming HC, Neu TR, Wozniak DJ. The EPS Matrix: The “House of Biofilm Cells.” J Bacteriol. 2007;189(22):7945–7. doi:10.1128/JB.00858-07
32. Flemming HC, Wingender J, Szewzyk U, Steinberg P, Rice SA, Kjelleberg S. Biofilms: an emergent form of bacterial life. Nat Rev Microbiol. 2016;14(9):563–75. doi:10.1038/nrmicro.2016.94
33. Gao X, Zhang H, Zhang X, Zhang C, Mao C, Shan S, et al. Interactions between extracellular polymeric substances and engineered nanoparticles in aquatic systems and their environmental effects: a comprehensive review. Environ Sci Nano. 2025;12(4):2177–92. doi:10.1039/D5EN00073D
34. Wang S, Peng Y. Natural zeolites as effective adsorbents in water and wastewater treatment. Chem Eng J. 2010;156(1):11–24. doi:10.1016/j.cej.2009.10.029
35. Ateia M, Alalm MG, Awfa D, Johnson MS, Yoshimura C. Modeling the degradation and disinfection of water pollutants by photocatalysts and composites: A critical review. Sci Total Environ. 2020;698:134197. doi:10.1016/j.scitotenv.2019.134197
36. Bloh JZ. Intensification of Heterogeneous Photocatalytic Reactions Without Efficiency Losses: The Importance of Surface Catalysis. Catal Lett. 2021;151(11):3105–13. doi:10.1007/s10562-021-03573-0

37. Sun Z, Wang S, Hu X. Polymer-Functionalized Nanocatalysts: Engineering Interfaces and Microenvironments for Enhanced Catalysis. Polymers. 2026;18(4):465. doi:10.3390/polym18040465
38. Tran HD, Nguyen DQ, Do PT, Tran UNP. Kinetics of photocatalytic degradation of organic compounds: a mini-review and new approach. RSC Adv. 2023;13(25):16915–25. doi:10.1039/D3RA01970E
39. AlMohamadi H, Awad SA, Sharma AK, Fayzullaev N, Távara-Aponte A, Chiguala-Contreras L, et al. Photocatalytic Activity of Metal- and Non-Metal-Anchored ZnO and TiO2 Nanocatalysts for Advanced Photocatalysis: Comparative Study. Catalysts. 2024;14(7):420. doi:10.3390/catal14070420
40. Chen D, Cheng Y, Zhou N, Chen P, Wang Y, Li K, et al. Photocatalytic degradation of organic pollutants using TiO2-based photocatalysts: A review. J Clean Prod. 2020;268:121725. doi:10.1016/j.jclepro.2020.121725
41. Navidpour AH, Hosseinzadeh A, Zhou JL, Huang Z. Progress in the application of surface engineering methods in immobilizing TiO_2 and ZnO coatings for environmental photocatalysis. Catal Rev. 2023;65(3):822–73. doi:10.1080/01614940.2021.1983066
42. Xu YJ. Promises and Challenges in Photocatalysis. Front Catal. 2021;1:708319. doi:10.3389/fctls.2021.708319
43. Hmoudah M, Paparo R, Chianese C, El-Qanni A, Salmi T, Tesser R, et al. Ibuprofen photodegradation promoted by ZnO and TiO2-P25 nanoparticles: A comprehensive kinetic, reaction mechanisms, and thermodynamic investigation. J Water Process Eng. 2025;69:106598. doi:10.1016/j.jwpe.2024.106598
44. Paiu M, Lutic D, Favier L, Gavrilescu M. Heterogeneous Photocatalysis for Advanced Water Treatment: Materials, Mechanisms, Reactor Configurations, and Emerging Applications. Appl Sci. 2025;15(10):5681. doi:10.3390/app15105681
45. Pérez-Botella E, Valencia S, Rey F. Zeolites in Adsorption Processes: State of the Art and Future Prospects. Chem Rev. 2022;122(24):17647–95. doi:10.1021/acs.chemrev.2c00140
46. Mehta K, Shukla A, Saraf M. Articulating the exuberant intricacies of bacterial exopolysaccharides to purge environmental pollutants. Heliyon. 2021;7(11):e08446. doi:10.1016/j.heliyon.2021.e08446
47. Dueñas-Moreno J, Mora A, Cervantes-Avilés P, Mahlknecht J. Groundwater contamination pathways of phthalates and bisphenol A: origin, characteristics, transport, and fate – A review. Environ Int. 2022;170:107550. doi:10.1016/j.envint.2022.107550
48. Alazaiza MYD, Alzghoul TM, Farobie O, Al-Yazeedi AA, Amr SSA, Bashir MJK. Advanced Oxidation Processes in Water Treatment: Mapping 15 Years of Scientific Progress and Collaboration. Environments. 2026;13(2):103. doi:10.3390/environments13020103
49. Hahn CG, Malinga SP, Makhetha TA. Degradation of bisphenol A using a MOF@COF-modified polyacrylonitrile ultrafiltration membrane. Chem Eng J Adv. 2025;23:100822. doi:10.1016/j.ceja.2025.100822

50. Ahmad MR, Ansari AA, Dhayal M, Lv R. Bandgap engineering of ZnO nanomaterials for enhanced electrochemical and photocatalytic efficiency. Renew Sustain Energy Rev. 2025;219:115767. doi:10.1016/j.rser.2025.115767
51. Debroy A, Sinha AK, Maity C, Pulimi M, Peijnenburg WJGM, Mukherjee A. In-situ and ex-situ EPS-corona formation on ZnO QDs mitigates their environmental toxicity in the freshwater microalgae Chlorella sp. J Hazard Mater. 2025;486:137034. doi:10.1016/j.jhazmat.2024.137034

Figures

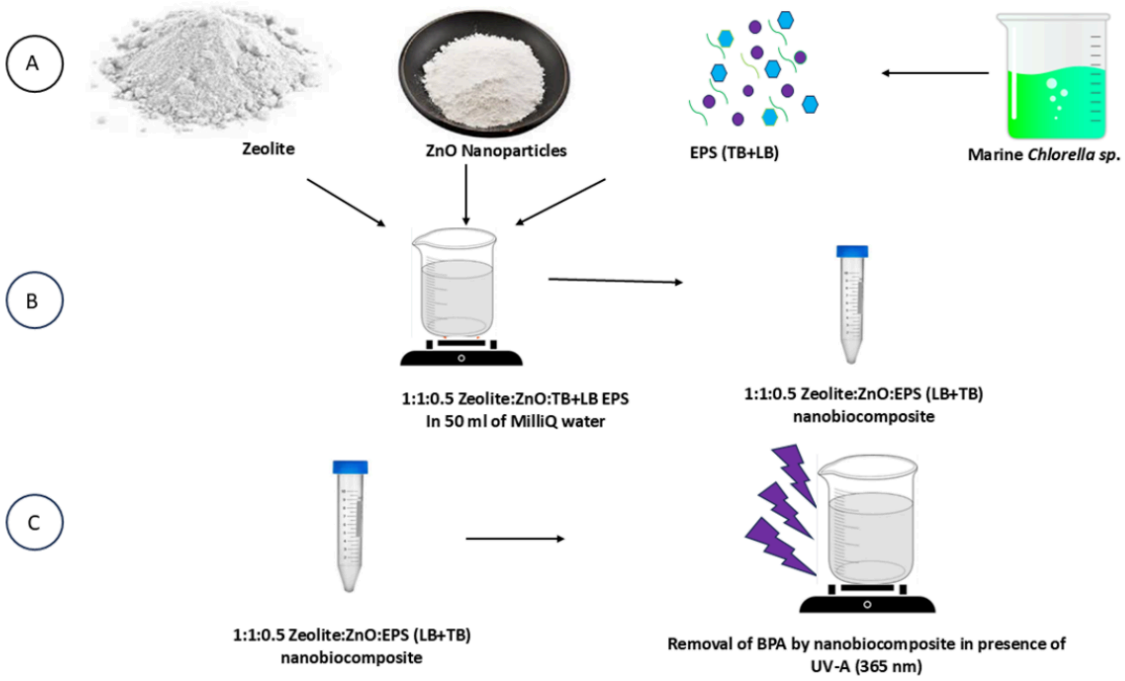


Figure 1

Schematic diagram of (A) preparation of chemicals, (B) synthesis of the bio-nanocomposite, and (C) BPA removal process.

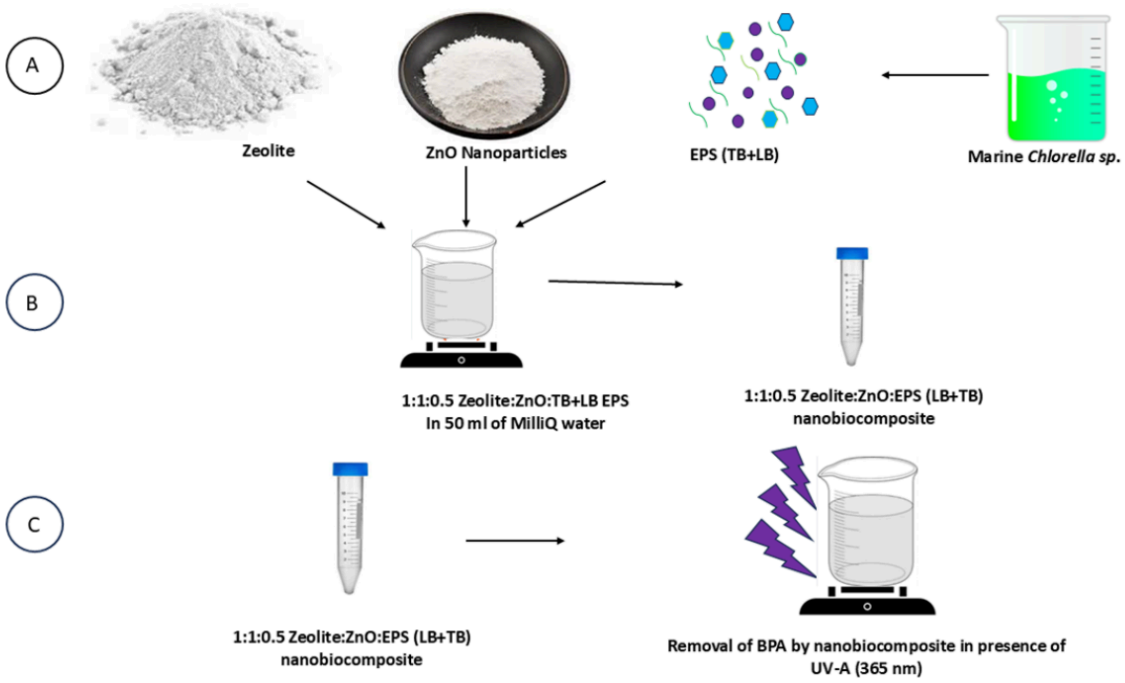


Figure 1

Schematic diagram of (A) preparation of chemicals, (B) synthesis of the bio-nanocomposite, and (C) BPA removal process.

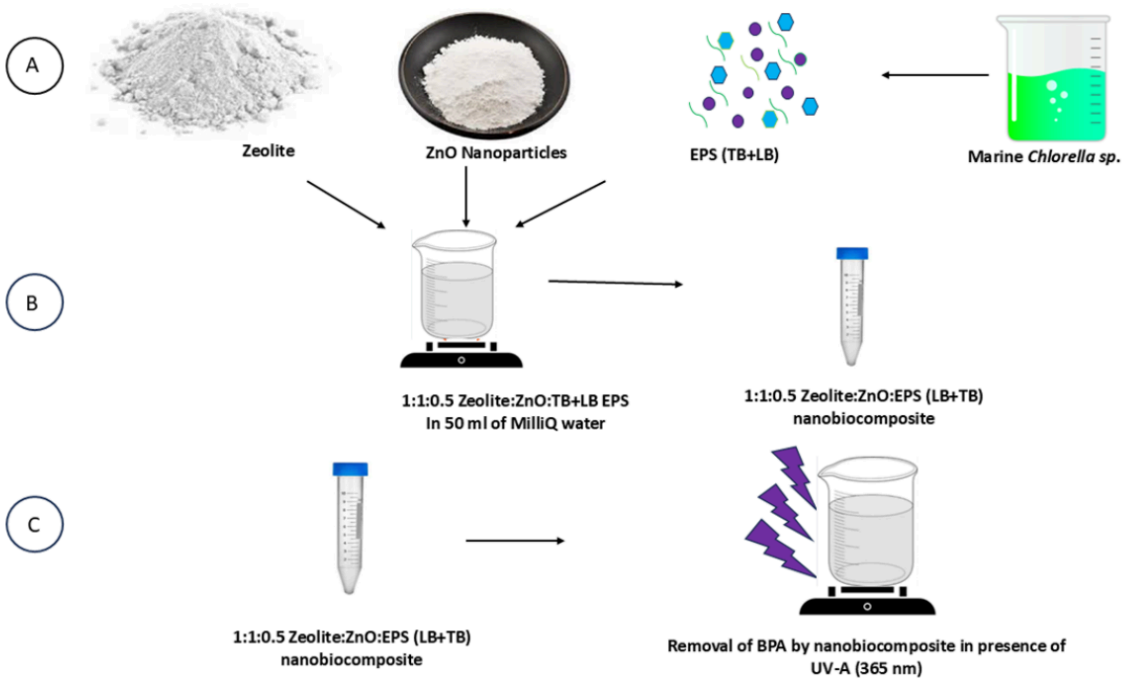


Figure 1

Schematic diagram of (A) preparation of chemicals, (B) synthesis of the bio-nanocomposite, and (C) BPA removal process.

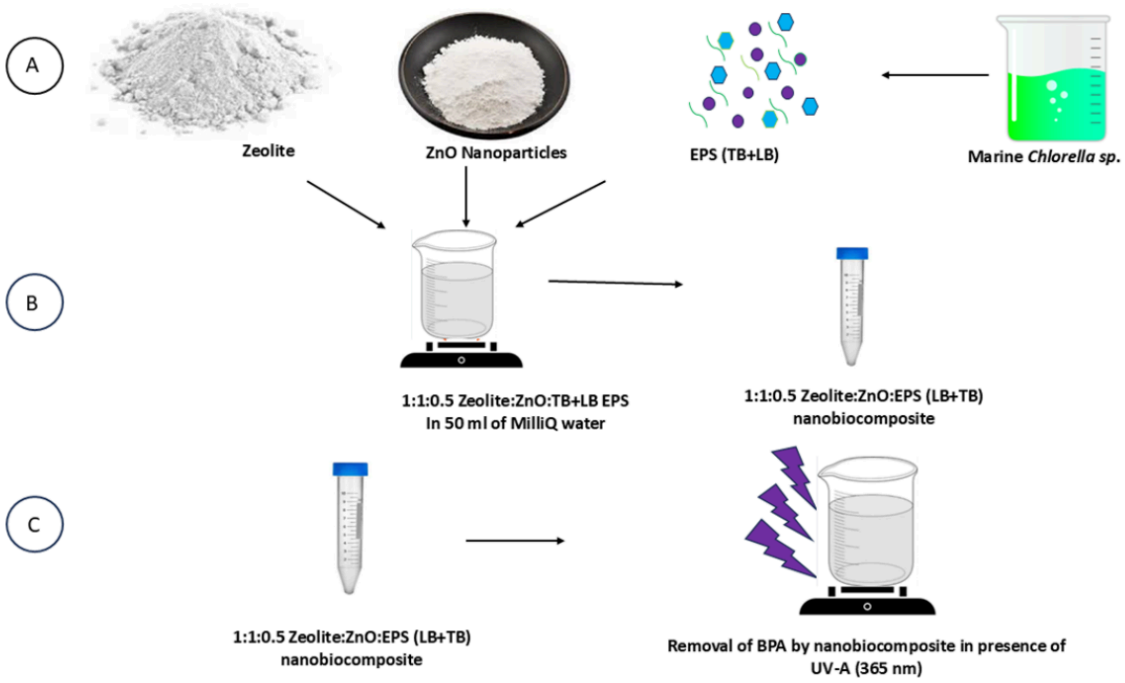


Figure 1

Schematic diagram of (A) preparation of chemicals, (B) synthesis of the bio-nanocomposite, and (C) BPA removal process.

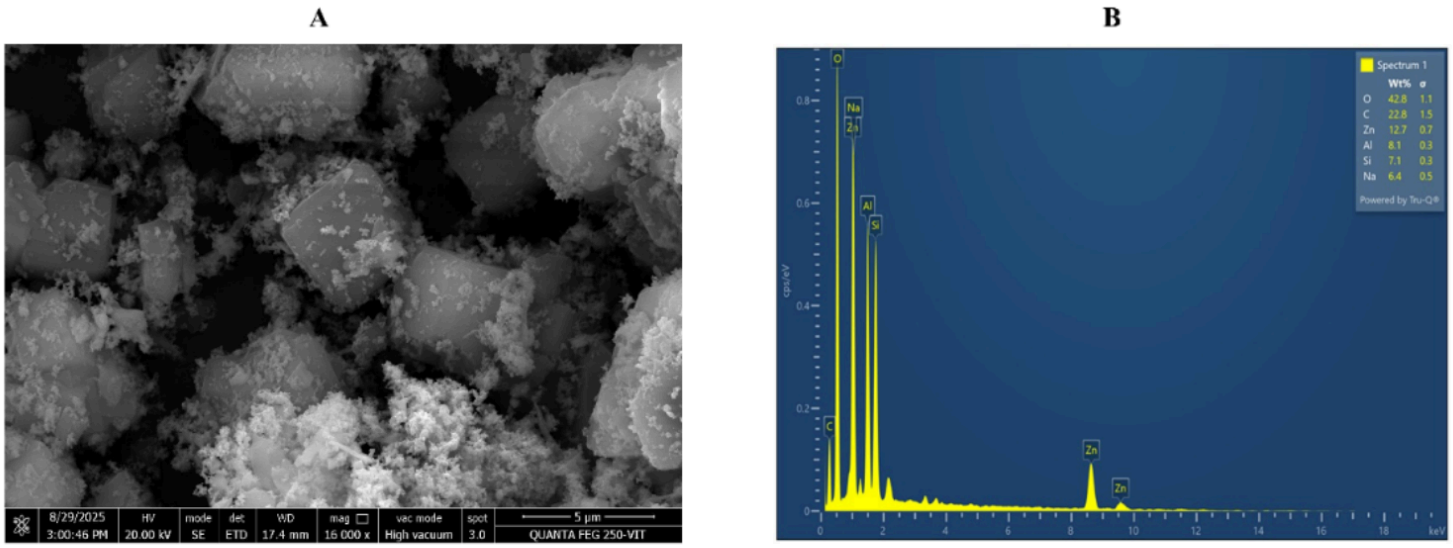


Figure 2

FE-SEM of the synthesized algal EPS based bio-nanocomposite (A) and the EDX spectra of Zeolite:ZnO:EPS bio-nanocomposite (B).

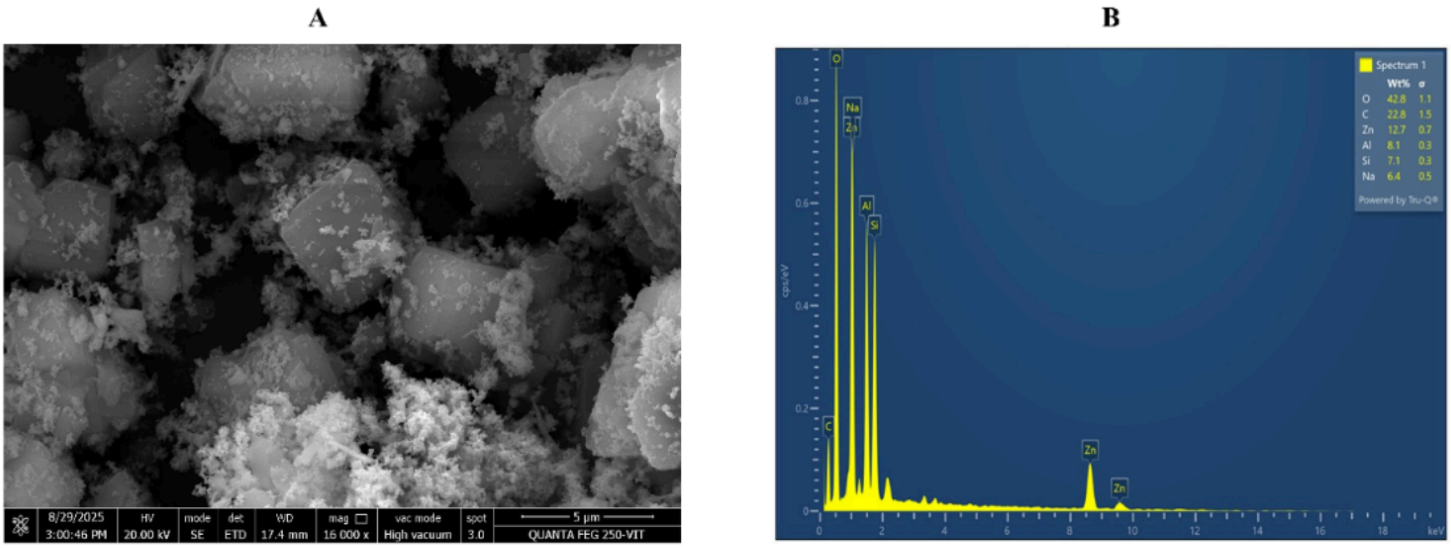


Figure 2

FE-SEM of the synthesized algal EPS based bio-nanocomposite (A) and the EDX spectra of Zeolite:ZnO:EPS bio-nanocomposite (B).

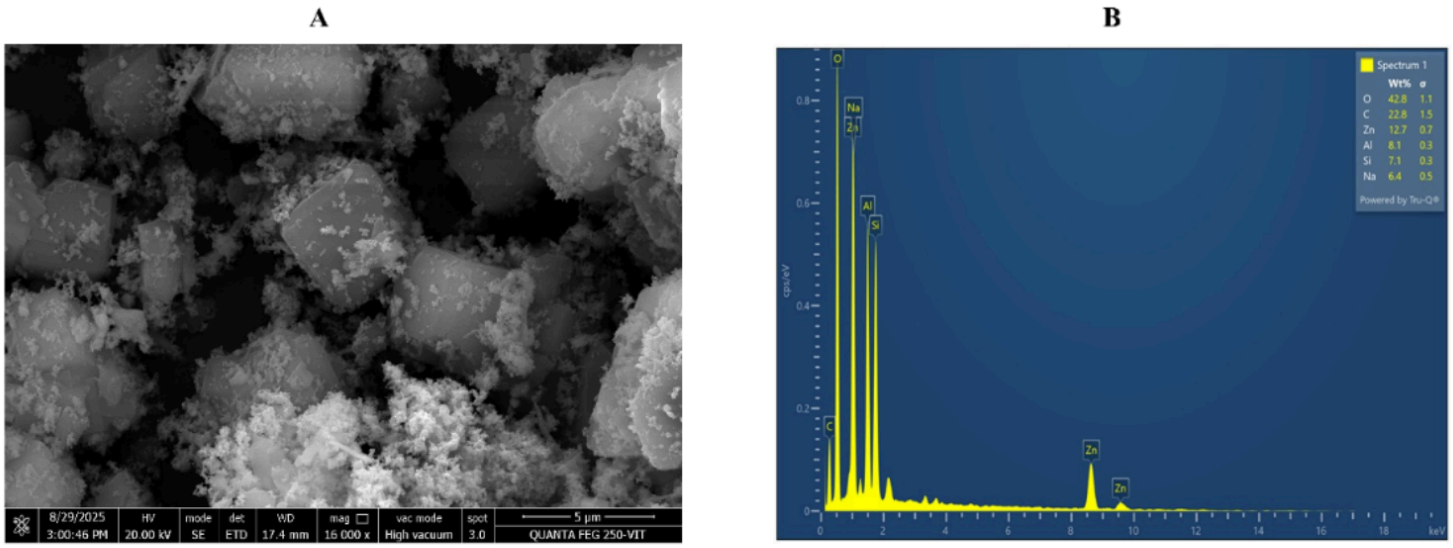


Figure 2

FE-SEM of the synthesized algal EPS based bio-nanocomposite (A) and the EDX spectra of Zeolite:ZnO:EPS bio-nanocomposite (B).

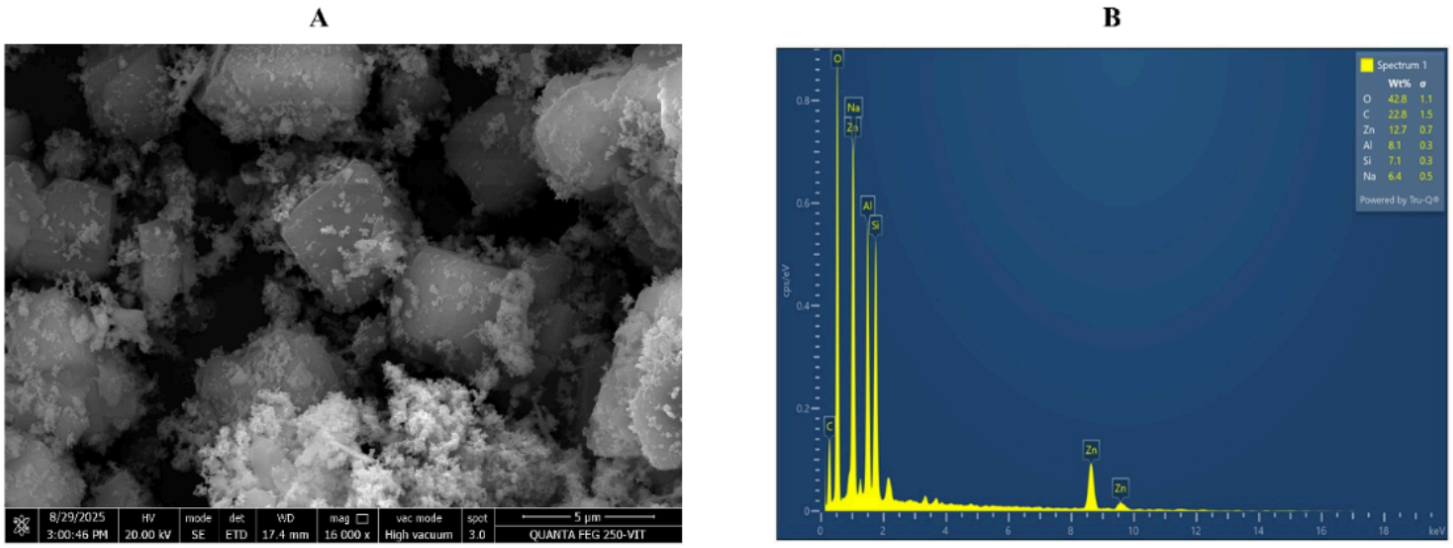


Figure 2

FE-SEM of the synthesized algal EPS based bio-nanocomposite (A) and the EDX spectra of Zeolite:ZnO:EPS bio-nanocomposite (B).

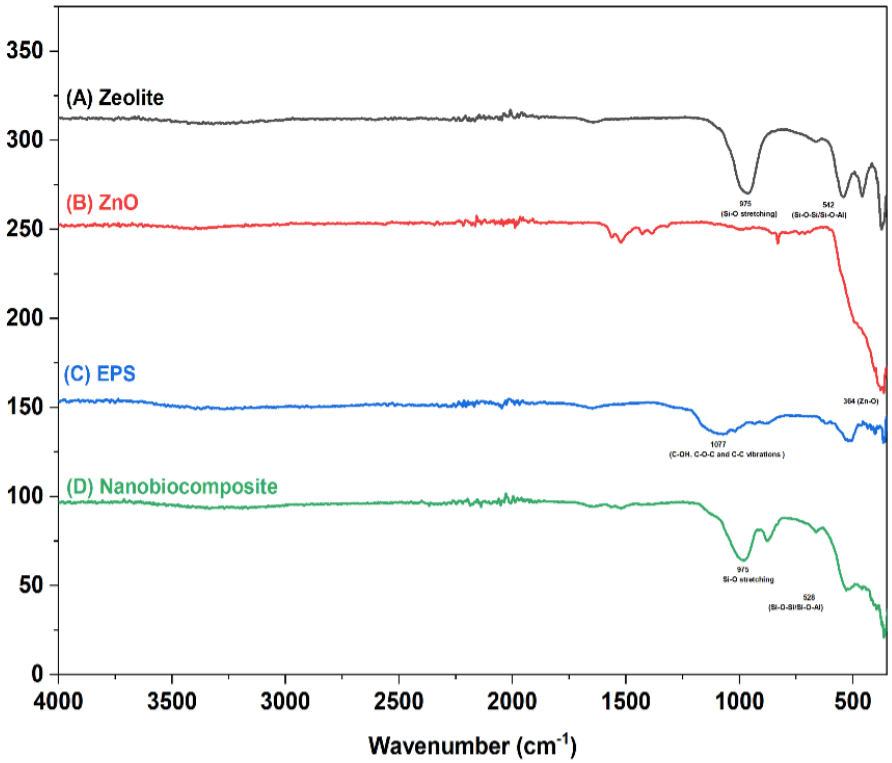


Figure 3

Fourier Transform Infrared (FTIR) spectroscopy analysis for Zeolite (A), ZnO (B), EPS (C) and Zeolite-ZnO-EPS bio-nanocomposite (D).

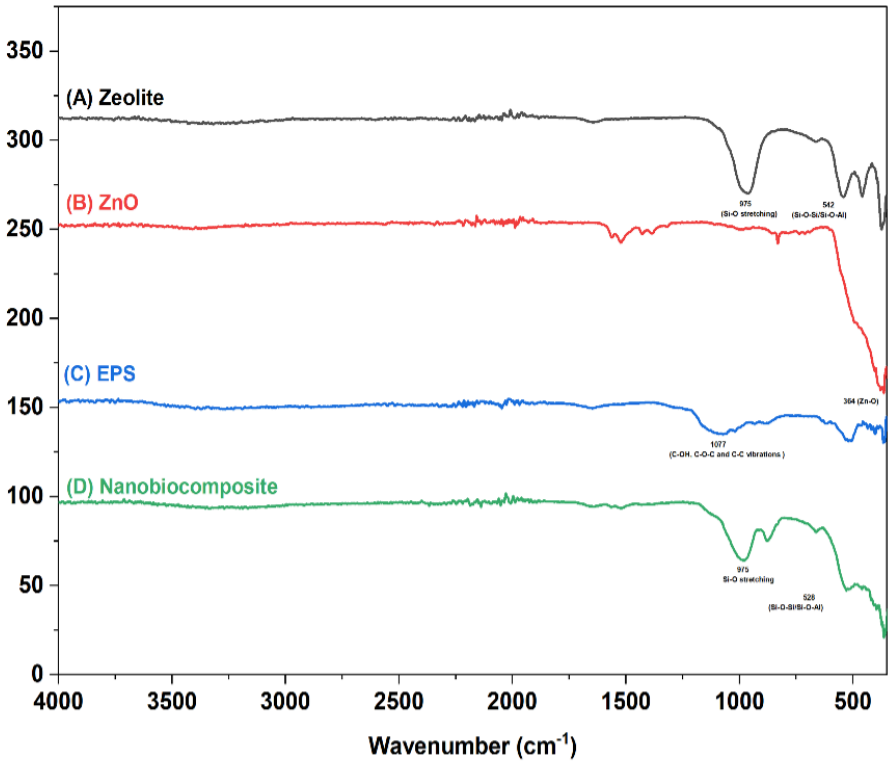


Figure 3

Fourier Transform Infrared (FTIR) spectroscopy analysis for Zeolite (A), ZnO (B), EPS (C) and Zeolite-ZnO-EPS bio-nanocomposite (D).

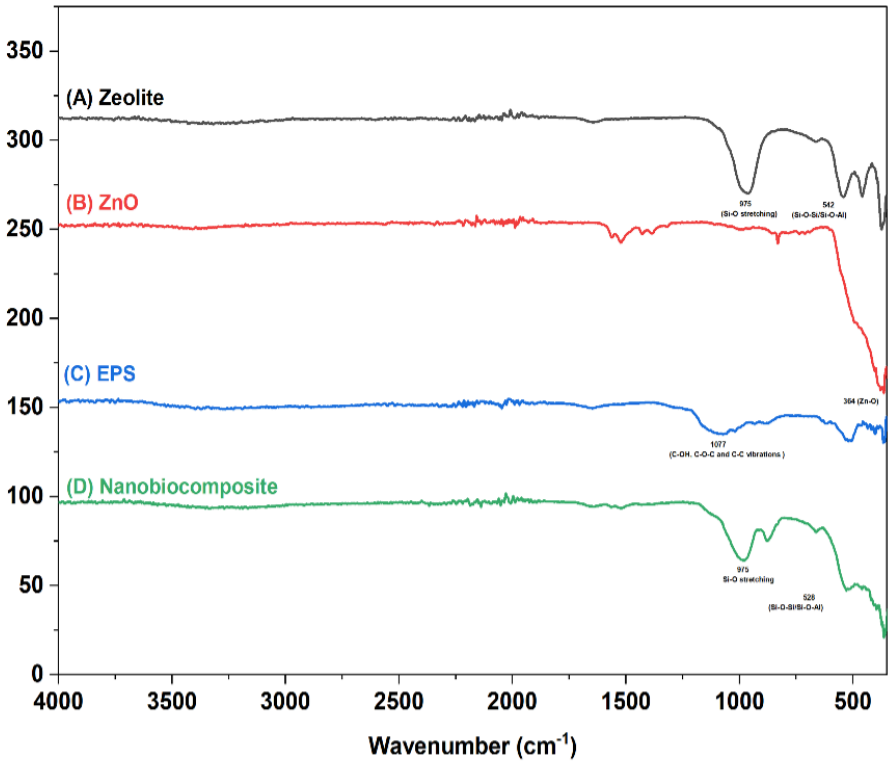


Figure 3

Fourier Transform Infrared (FTIR) spectroscopy analysis for Zeolite (A), ZnO (B), EPS (C) and Zeolite-ZnO-EPS bio-nanocomposite (D).

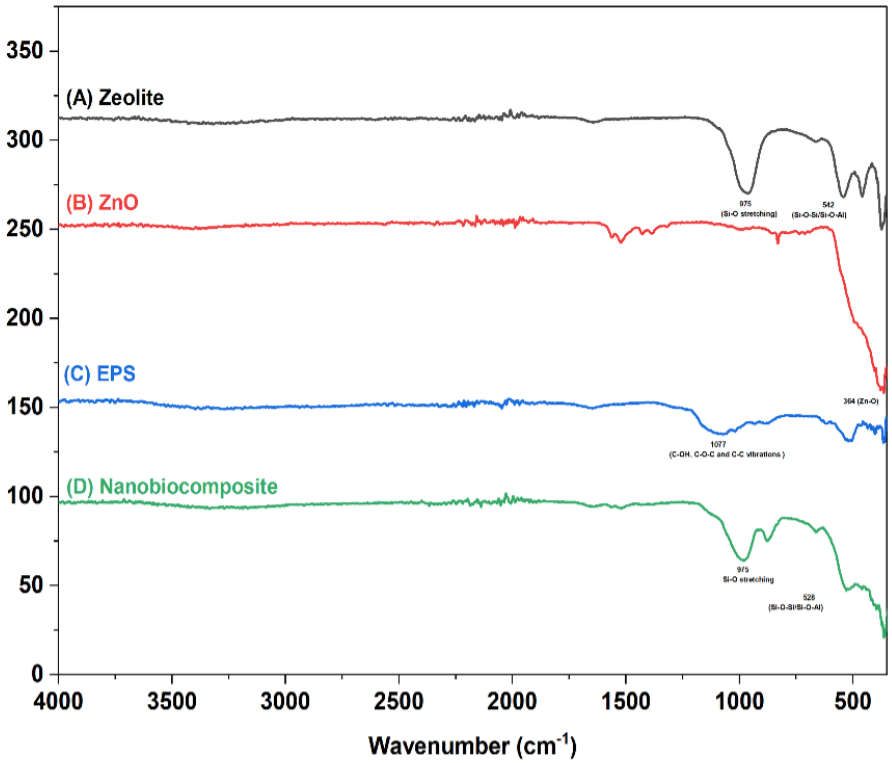


Figure 3

Fourier Transform Infrared (FTIR) spectroscopy analysis for Zeolite (A), ZnO (B), EPS (C) and Zeolite-ZnO-EPS bio-nanocomposite (D).

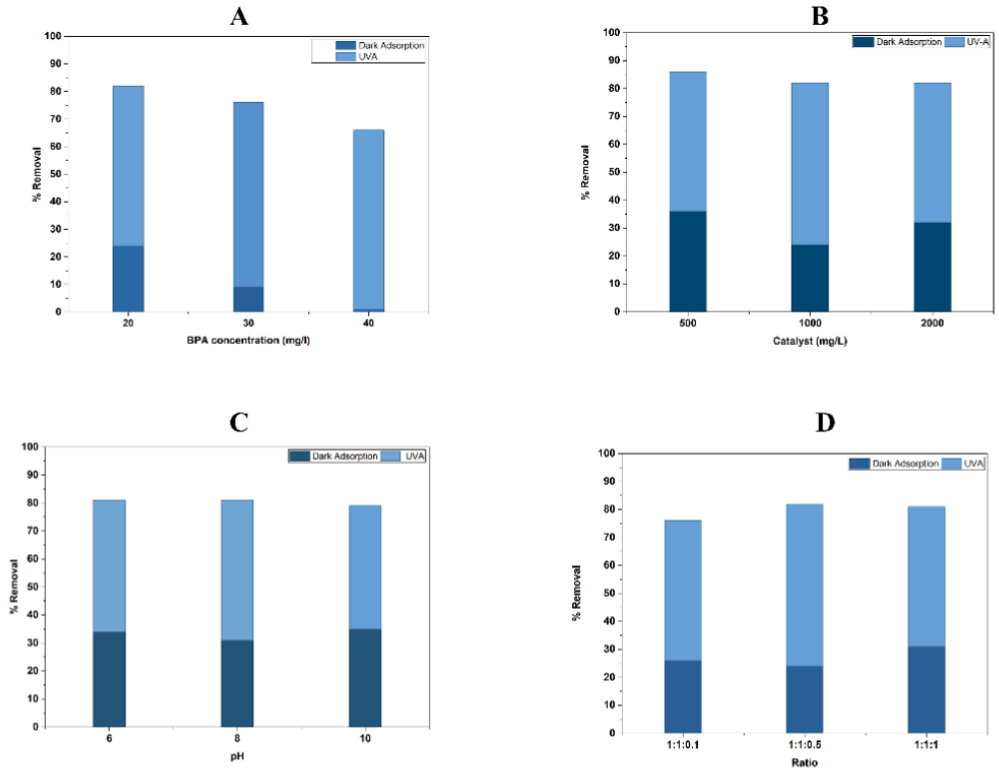


Figure 4

(A-C) Graphs for BPA removal studies, showing the effects of BPA concentration (A), catalyst dosage (B), and pH (C). (D) shows the optimization ratio of the bio-nanocomposite.

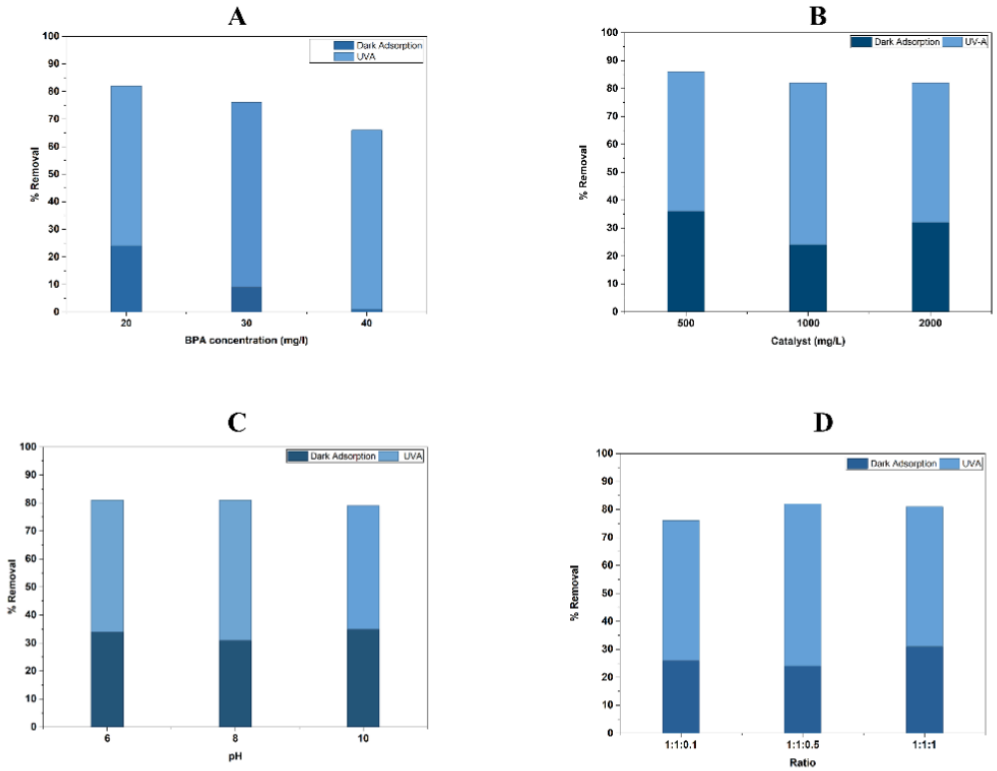


Figure 4

(A-C) Graphs for BPA removal studies, showing the effects of BPA concentration (A), catalyst dosage (B), and pH (C). (D) shows the optimization ratio of the bio-nanocomposite.

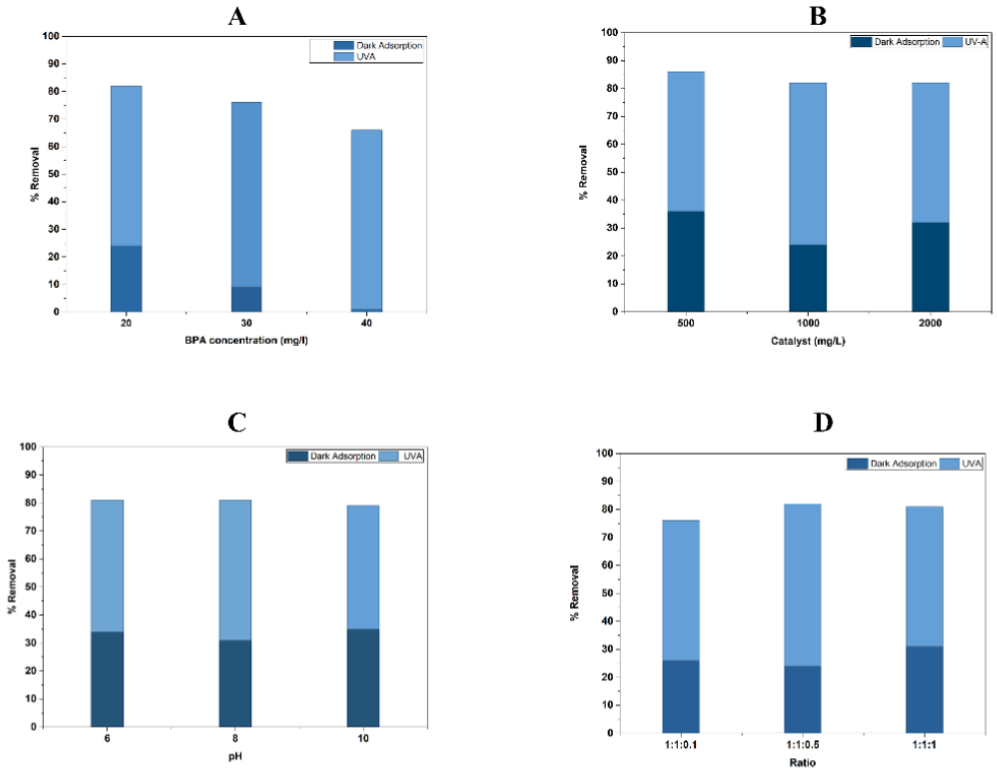


Figure 4

(A-C) Graphs for BPA removal studies, showing the effects of BPA concentration (A), catalyst dosage (B), and pH (C). (D) shows the optimization ratio of the bio-nanocomposite.

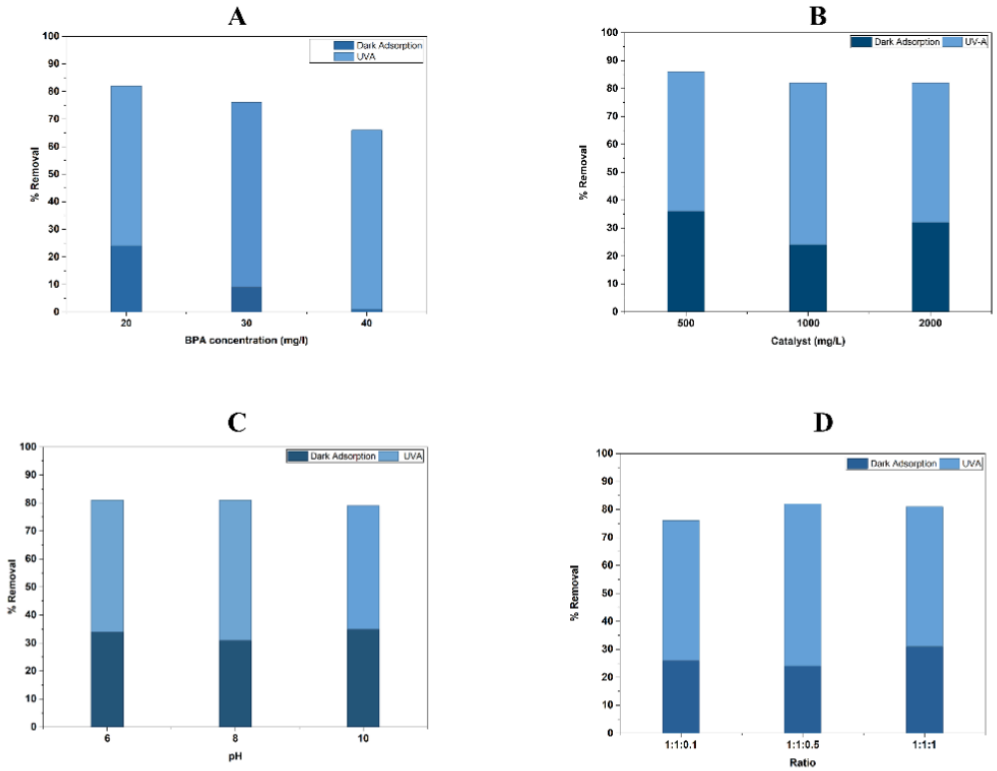


Figure 4

(A-C) Graphs for BPA removal studies, showing the effects of BPA concentration (A), catalyst dosage (B), and pH (C). (D) shows the optimization ratio of the bio-nanocomposite.

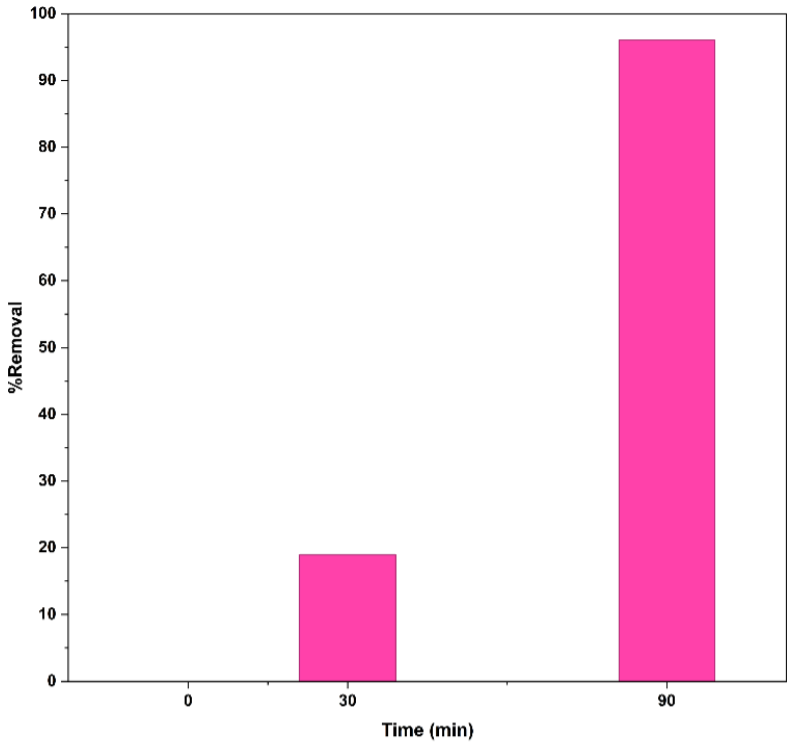


Figure 5

Extent of total organic carbon (TOC) removal during the degradation of bisphenol A (BPA) with respect to reaction time (0, 30, and 90 min).

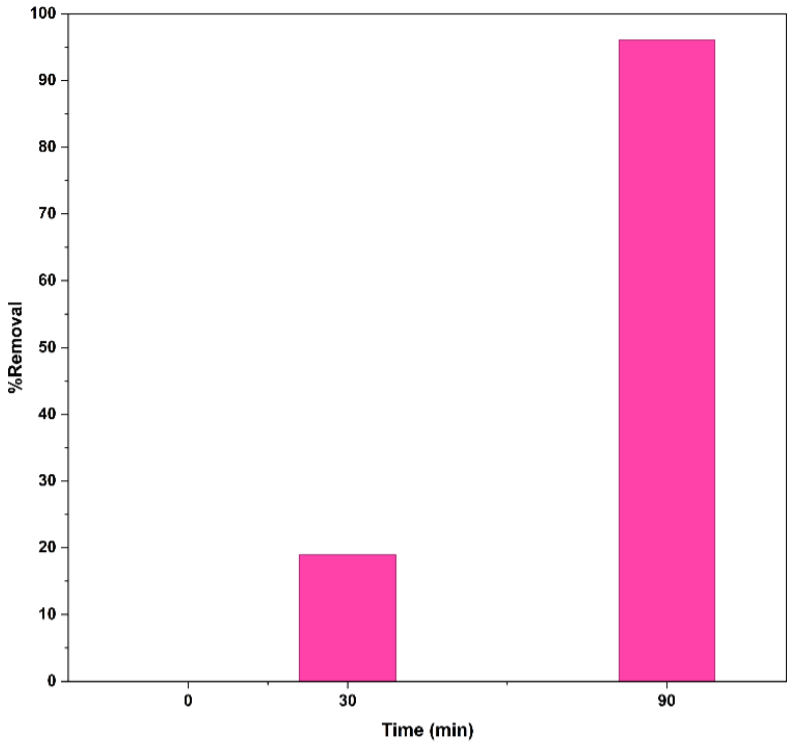


Figure 5

Extent of total organic carbon (TOC) removal during the degradation of bisphenol A (BPA) with respect to reaction time (0, 30, and 90 min).

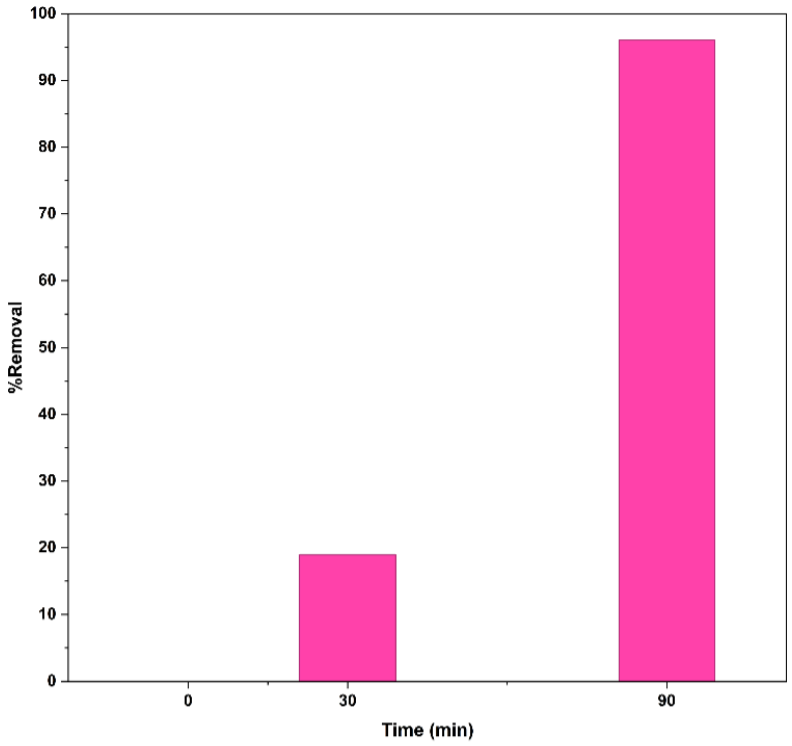


Figure 5

Extent of total organic carbon (TOC) removal during the degradation of bisphenol A (BPA) with respect to reaction time (0, 30, and 90 min).

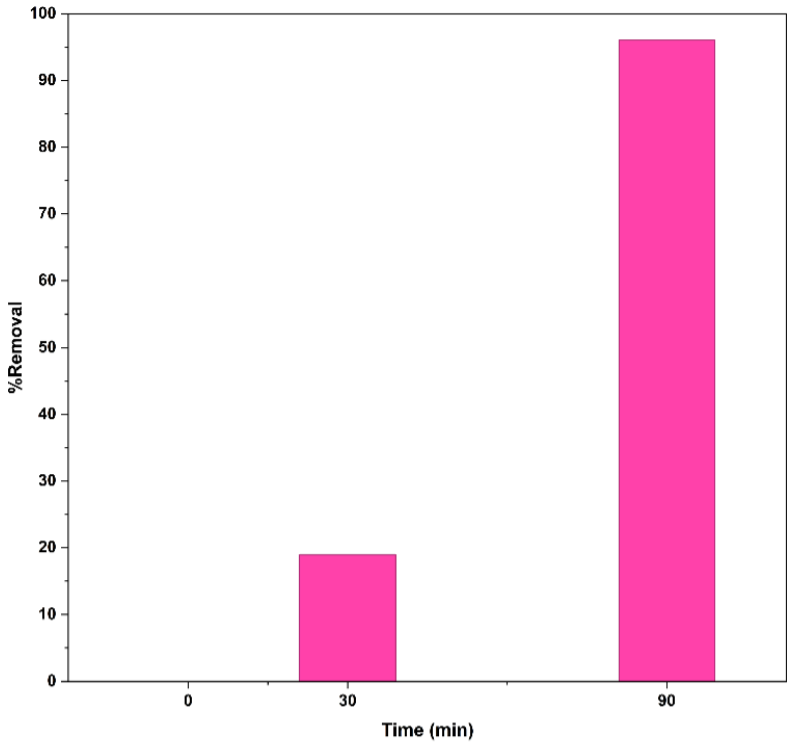


Figure 5

Extent of total organic carbon (TOC) removal during the degradation of bisphenol A (BPA) with respect to reaction time (0, 30, and 90 min).

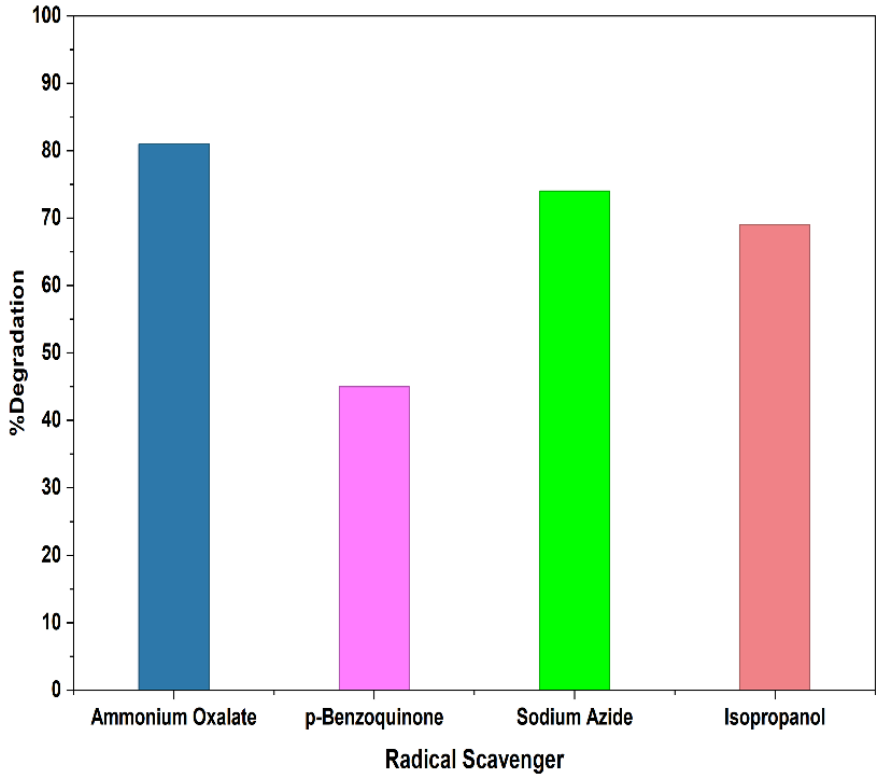


Figure 6

Effect of selective radical scavengers on the degradation efficiency of bisphenol A (BPA) to identify key reactive oxygen species (ROS)

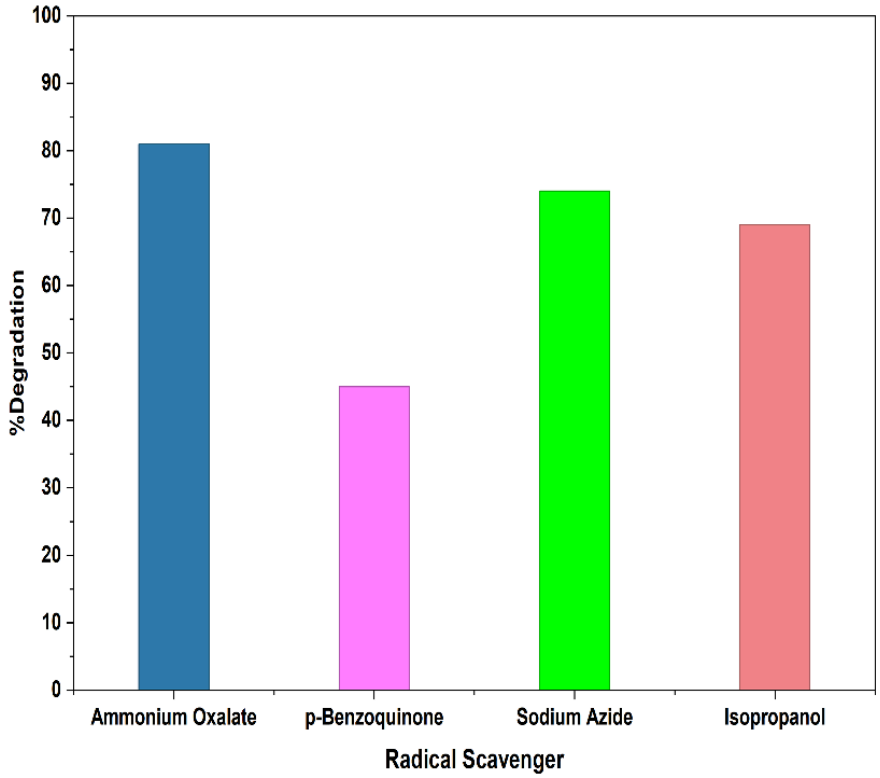


Figure 6

Effect of selective radical scavengers on the degradation efficiency of bisphenol A (BPA) to identify key reactive oxygen species (ROS)

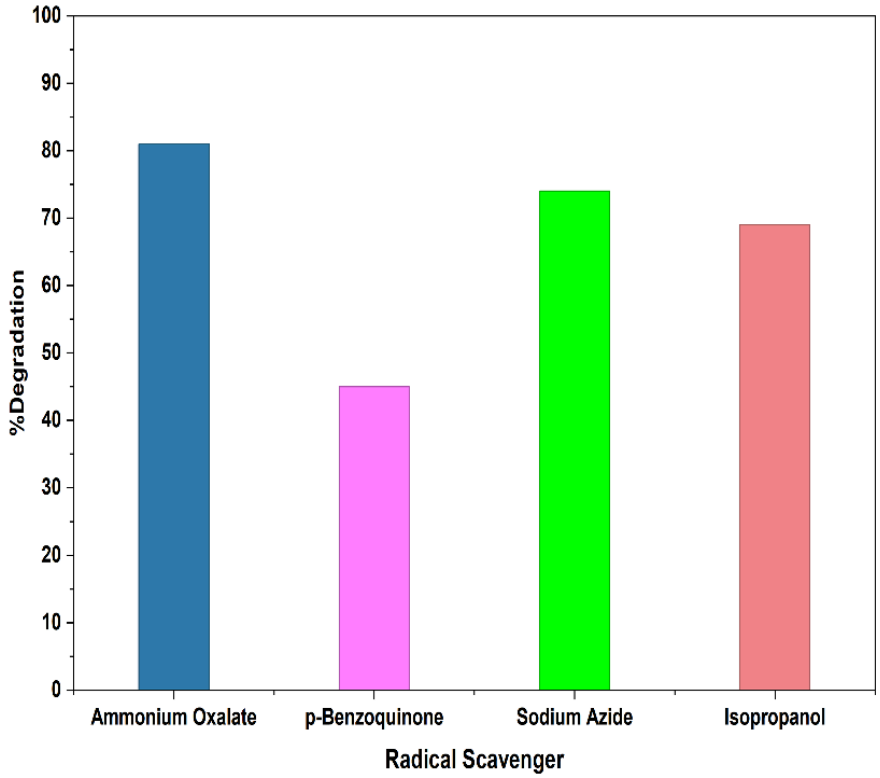


Figure 6

Effect of selective radical scavengers on the degradation efficiency of bisphenol A (BPA) to identify key reactive oxygen species (ROS)

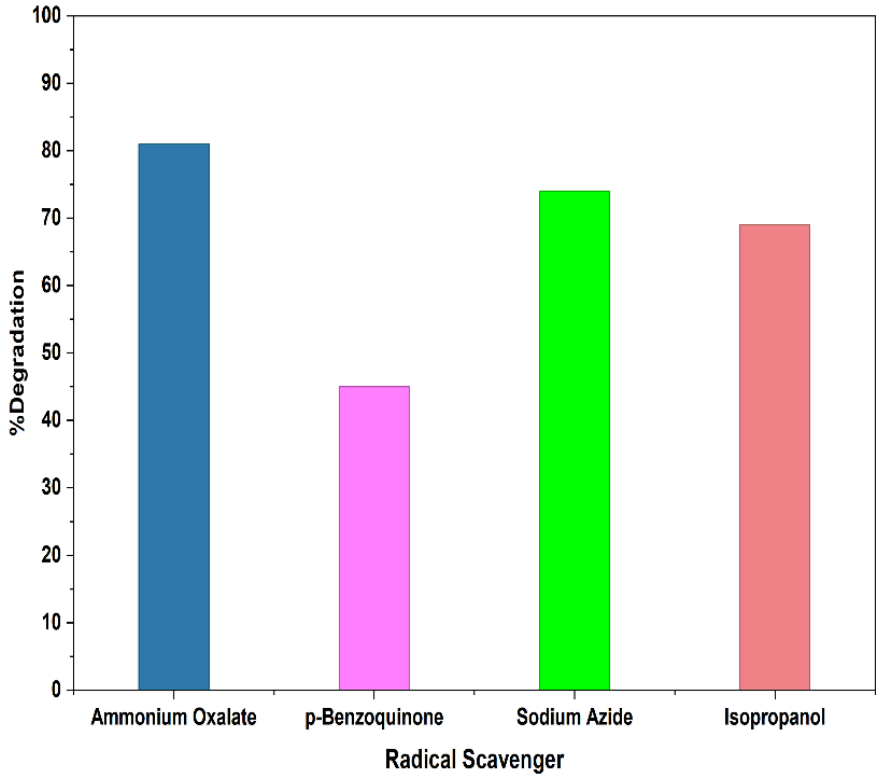


Figure 6

Effect of selective radical scavengers on the degradation efficiency of bisphenol A (BPA) to identify key reactive oxygen species (ROS)

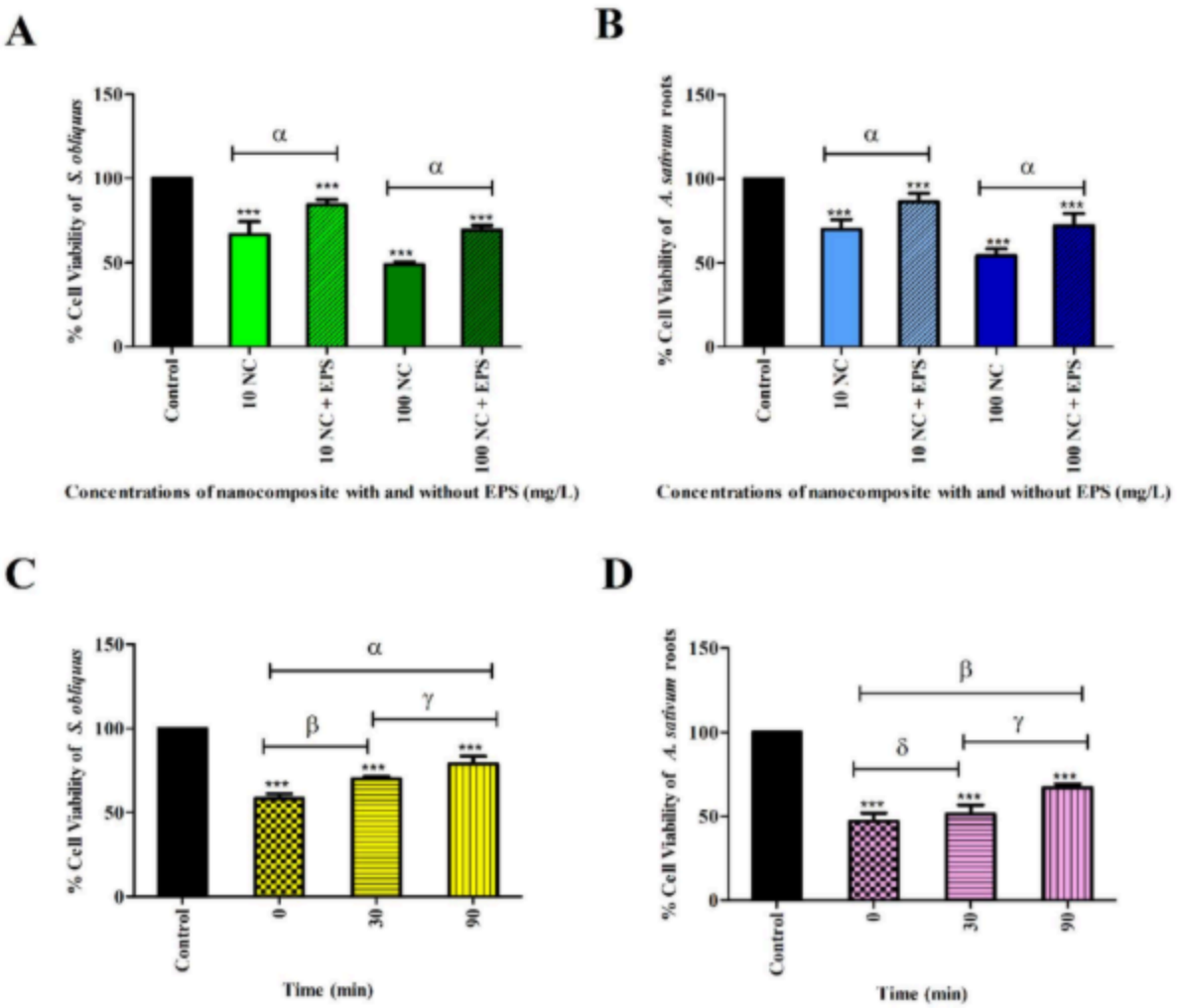


Figure 7

(A) Percentage cell viability of *Scenedesmus obliquus* exposed to Zeolite-ZnO NC with and without extracellular polymeric substances (EPS). (B) Percentage cell viability of *Allium sativum* roots exposed to nano Zeolite-ZnO NC with and without EPS. (C) Percentage cell viability of *Scenedesmus obliquus* following bisphenol A (BPA) removal. (D) Percentage cell viability of *Allium sativum* roots following BPA removal. The level of significance is shown by '***' ($p < 0.001$, 'α' $p < 0.001$, 'β'- $p < 0.01$, 'γ'- $p < 0.05$, and 'δ'- $p > 0.05$).

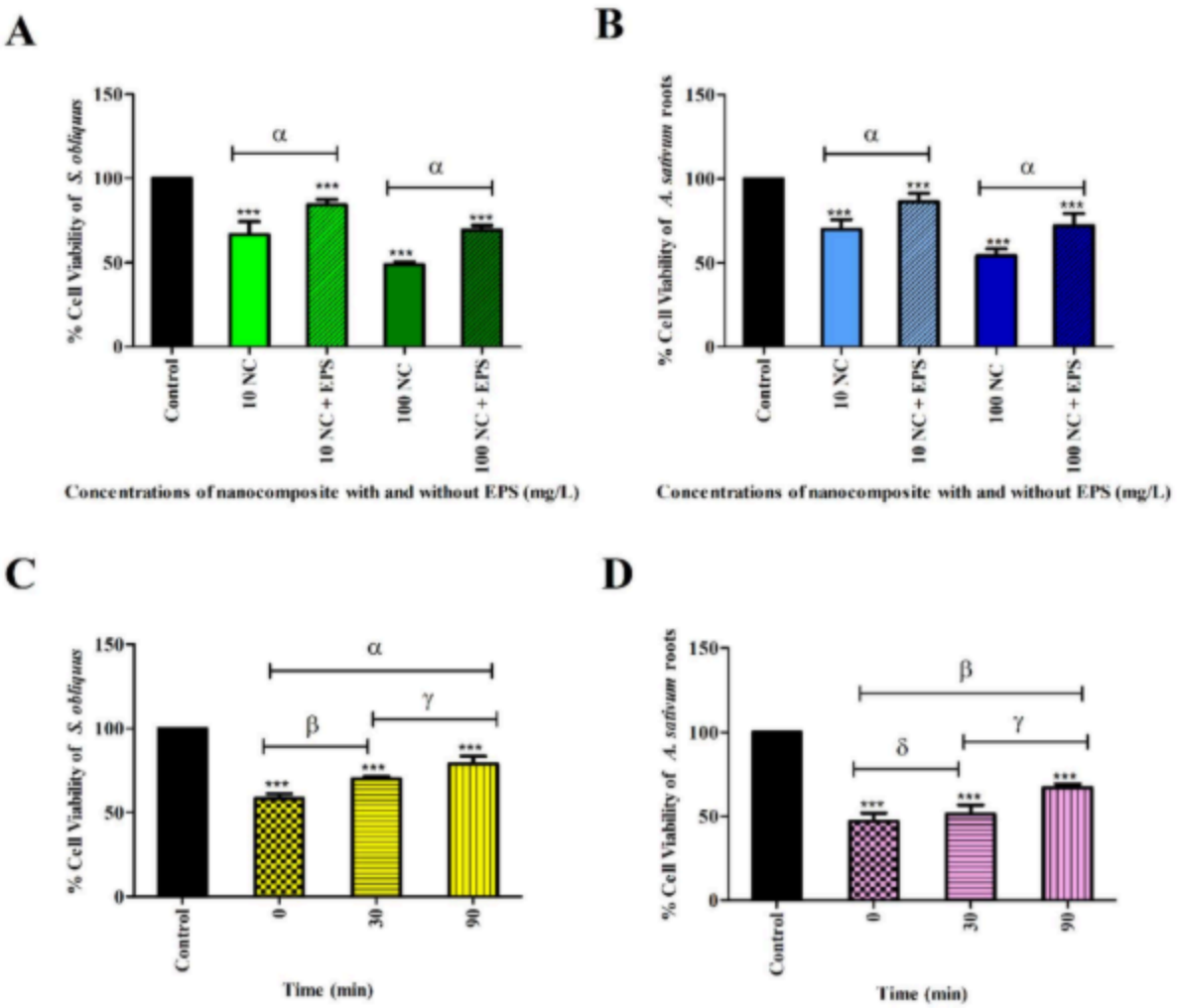


Figure 7

(A) Percentage cell viability of *Scenedesmus obliquus* exposed to Zeolite-ZnO NC with and without extracellular polymeric substances (EPS). (B) Percentage cell viability of *Allium sativum* roots exposed to nano Zeolite-ZnO NC with and without EPS. (C) Percentage cell viability of *Scenedesmus obliquus* following bisphenol A (BPA) removal. (D) Percentage cell viability of *Allium sativum* roots following BPA removal. The level of significance is shown by '***' ($p < 0.001$, 'α' $p < 0.001$, 'β'- $p < 0.01$, 'γ'- $p < 0.05$, and 'δ'- $p > 0.05$).

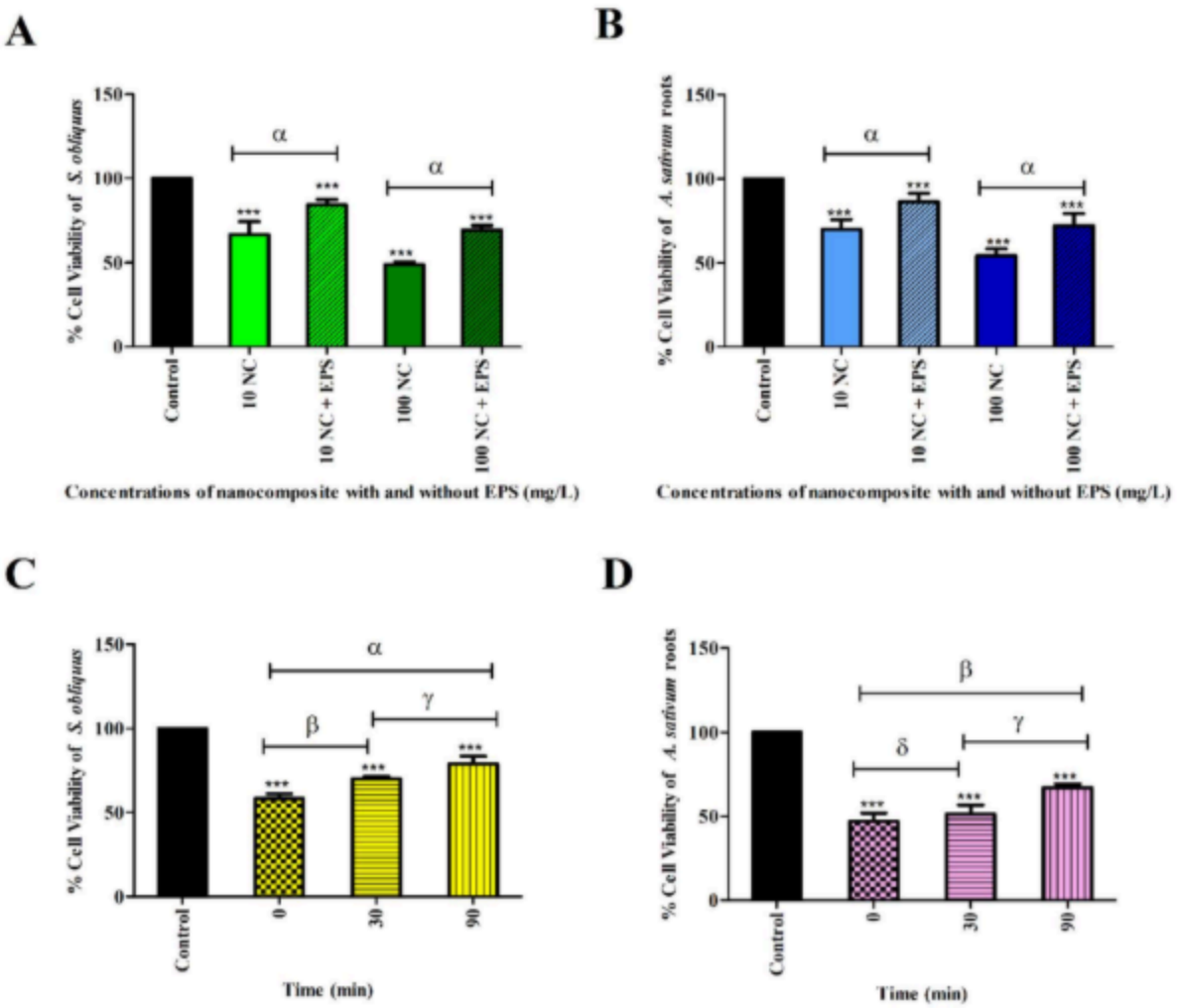


Figure 7

(A) Percentage cell viability of *Scenedesmus obliquus* exposed to Zeolite-ZnO NC with and without extracellular polymeric substances (EPS). (B) Percentage cell viability of *Allium sativum* roots exposed to nano Zeolite-ZnO NC with and without EPS. (C) Percentage cell viability of *Scenedesmus obliquus* following bisphenol A (BPA) removal. (D) Percentage cell viability of *Allium sativum* roots following BPA removal. The level of significance is shown by '***' ($p < 0.001$, 'α' $p < 0.001$, 'β'- $p < 0.01$, 'γ'- $p < 0.05$, and 'δ'- $p > 0.05$).

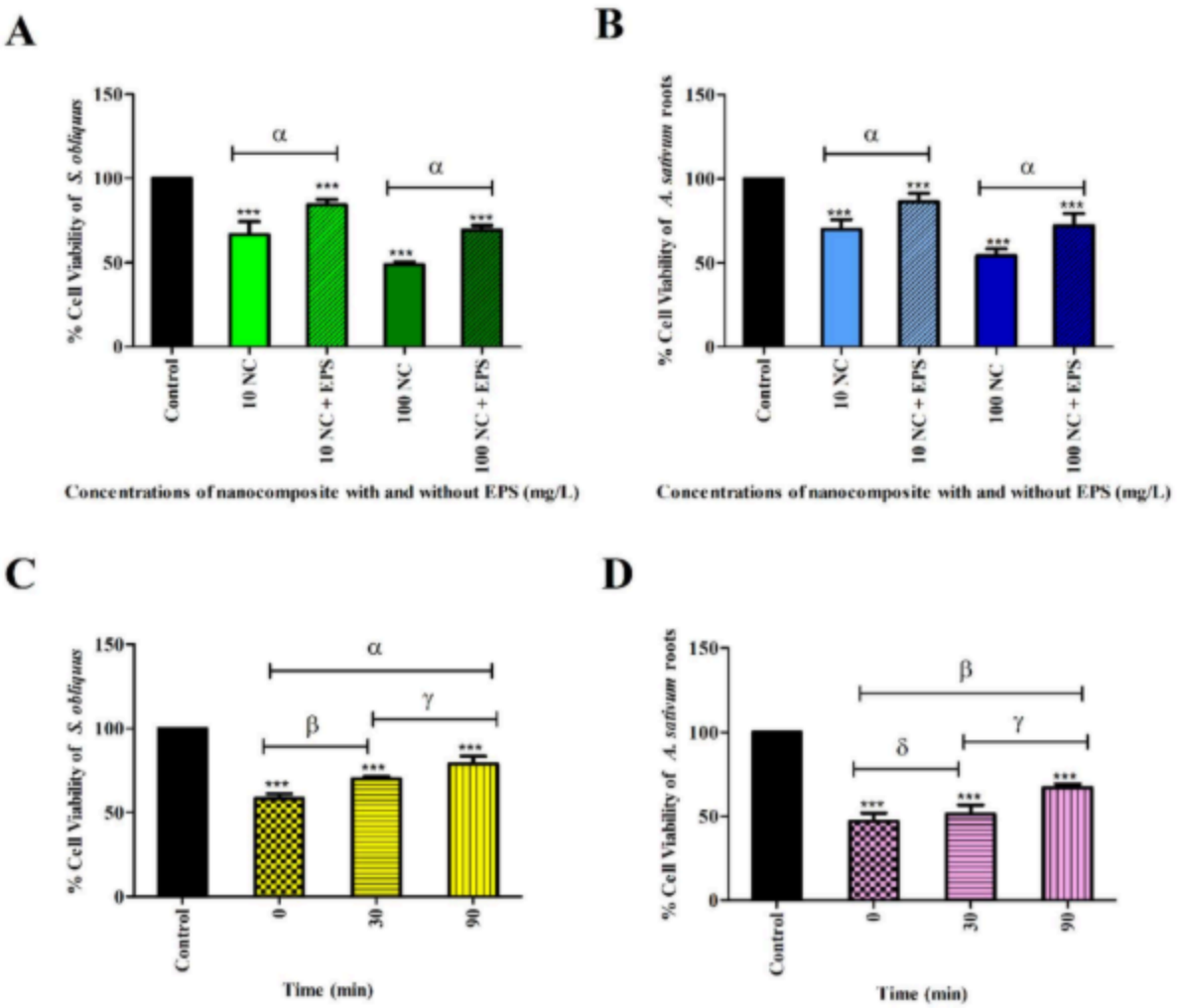


Figure 7

(A) Percentage cell viability of *Scenedesmus obliquus* exposed to Zeolite-ZnO NC with and without extracellular polymeric substances (EPS). (B) Percentage cell viability of *Allium sativum* roots exposed to nano Zeolite-ZnO NC with and without EPS. (C) Percentage cell viability of *Scenedesmus obliquus* following bisphenol A (BPA) removal. (D) Percentage cell viability of *Allium sativum* roots following BPA removal. The level of significance is shown by '***' ($p < 0.001$, 'α' $p < 0.001$, 'β'- $p < 0.01$, 'γ'- $p < 0.05$, and 'δ'- $p > 0.05$).

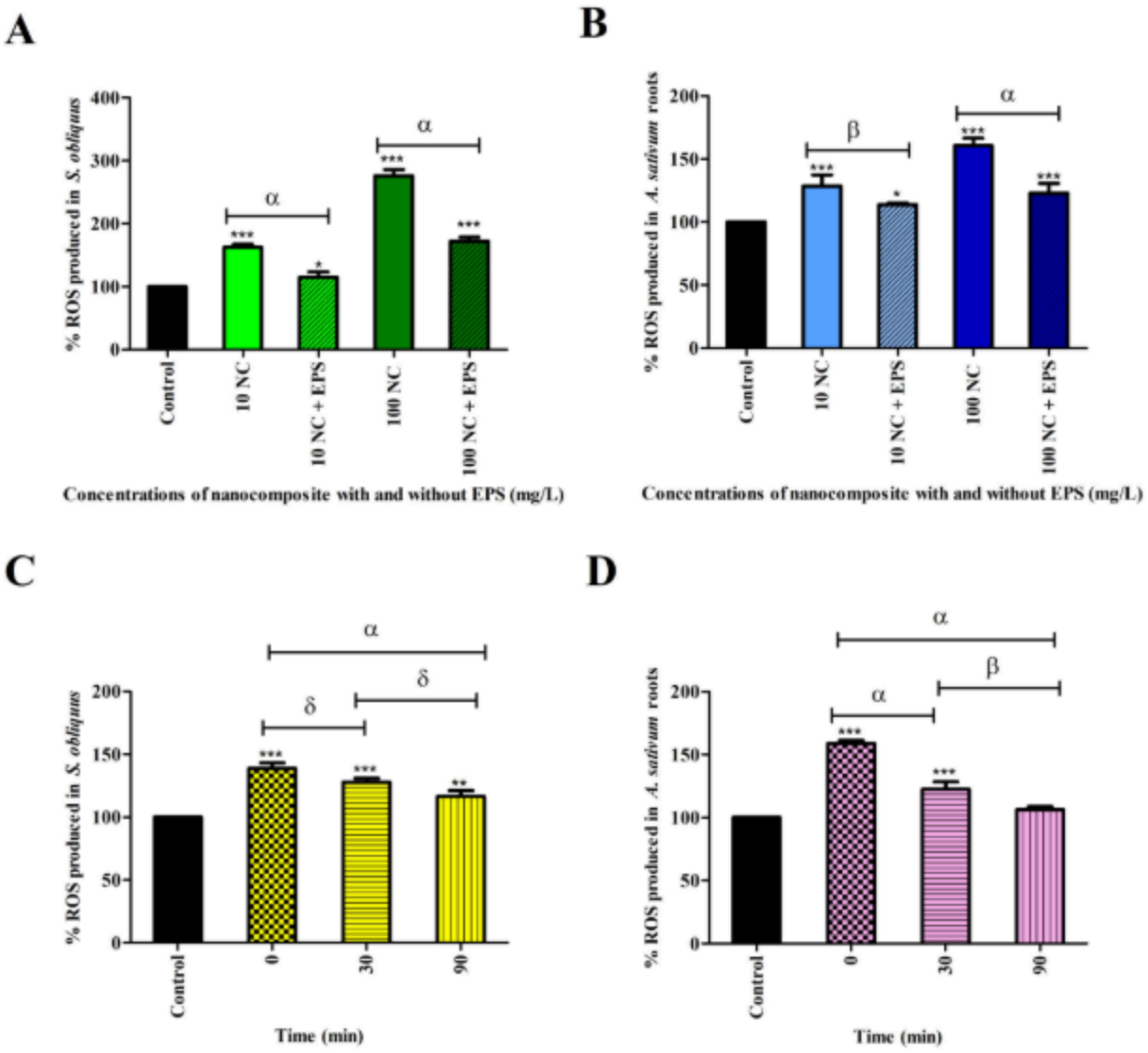


Figure 8

(A) Reactive oxygen species (ROS) production in the cells of *Scenedesmus obliquus* exposed to nano zinc oxide-zeolite nanocomposites (NC) with and without extracellular polymeric substances (EPS). (B) % ROS production in *Allium sativum* roots exposed to nano zinc oxide-zeolite NC with and without EPS. (C) % ROS production in *Scenedesmus obliquus* cells following bisphenol A (BPA) removal. (D) % ROS production in *Allium sativum* roots following BPA removal. The level of significance between the treatment vs control groups is shown by '***'-$p < 0.001$, '**'-$p < 0.01$, and '*'-$p < 0.05$, and between the treated groups is shown by 'α'- $p < 0.001$, 'β'- $p < 0.01$, and 'δ'- $p > 0.05$.

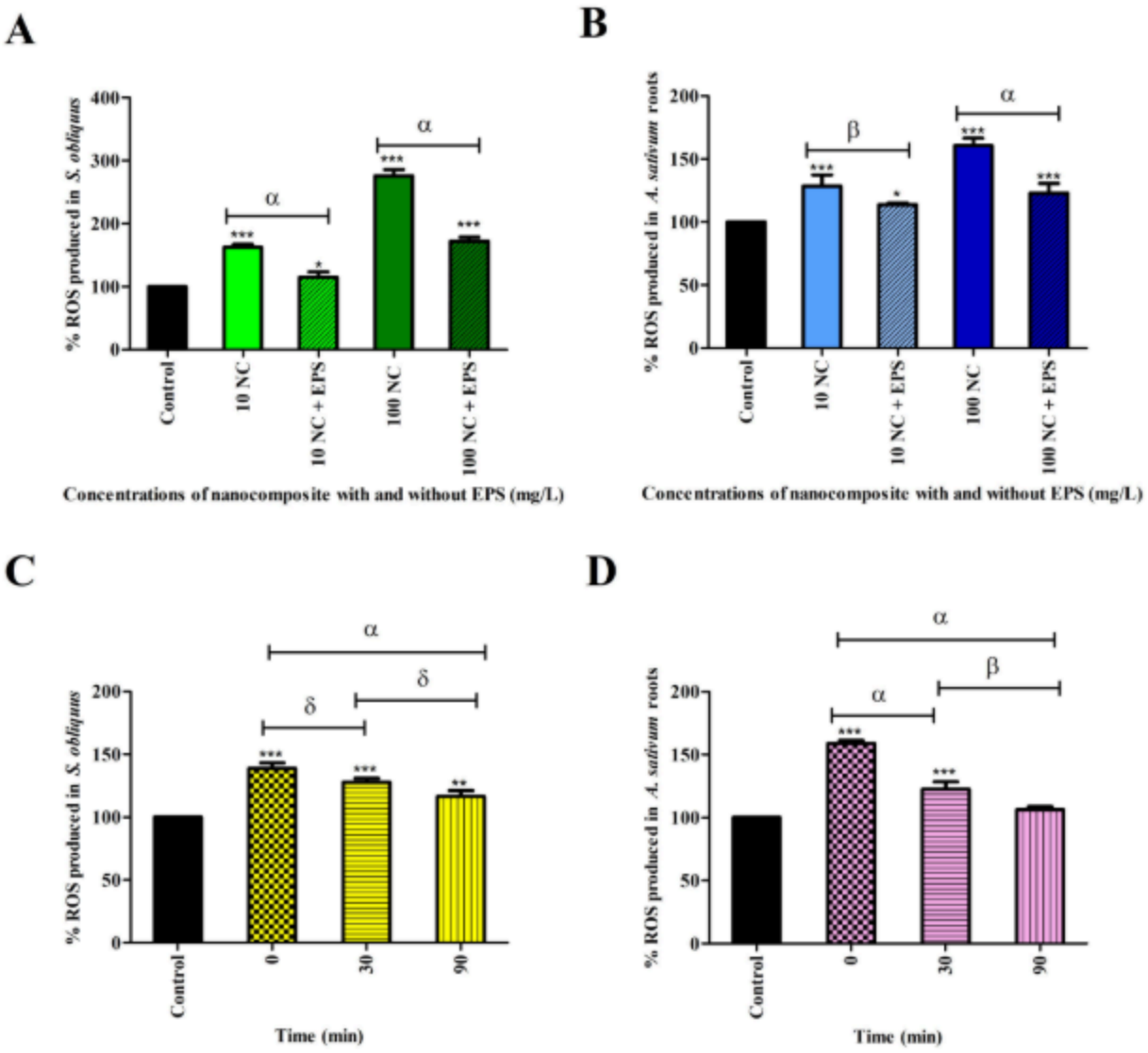


Figure 8

(A) Reactive oxygen species (ROS) production in the cells of *Scenedesmus obliquus* exposed to nano zinc oxide-zeolite nanocomposites (NC) with and without extracellular polymeric substances (EPS). (B) % ROS production in *Allium sativum* roots exposed to nano zinc oxide-zeolite NC with and without EPS. (C) % ROS production in *Scenedesmus obliquus* cells following bisphenol A (BPA) removal. (D) % ROS production in *Allium sativum* roots following BPA removal. The level of significance between the treatment vs control groups is shown by '***'-$p < 0.001$, '**'-$p < 0.01$, and '*'-$p < 0.05$, and between the treated groups is shown by 'α'- $p < 0.001$, 'β'- $p < 0.01$, and 'δ'- $p > 0.05$.

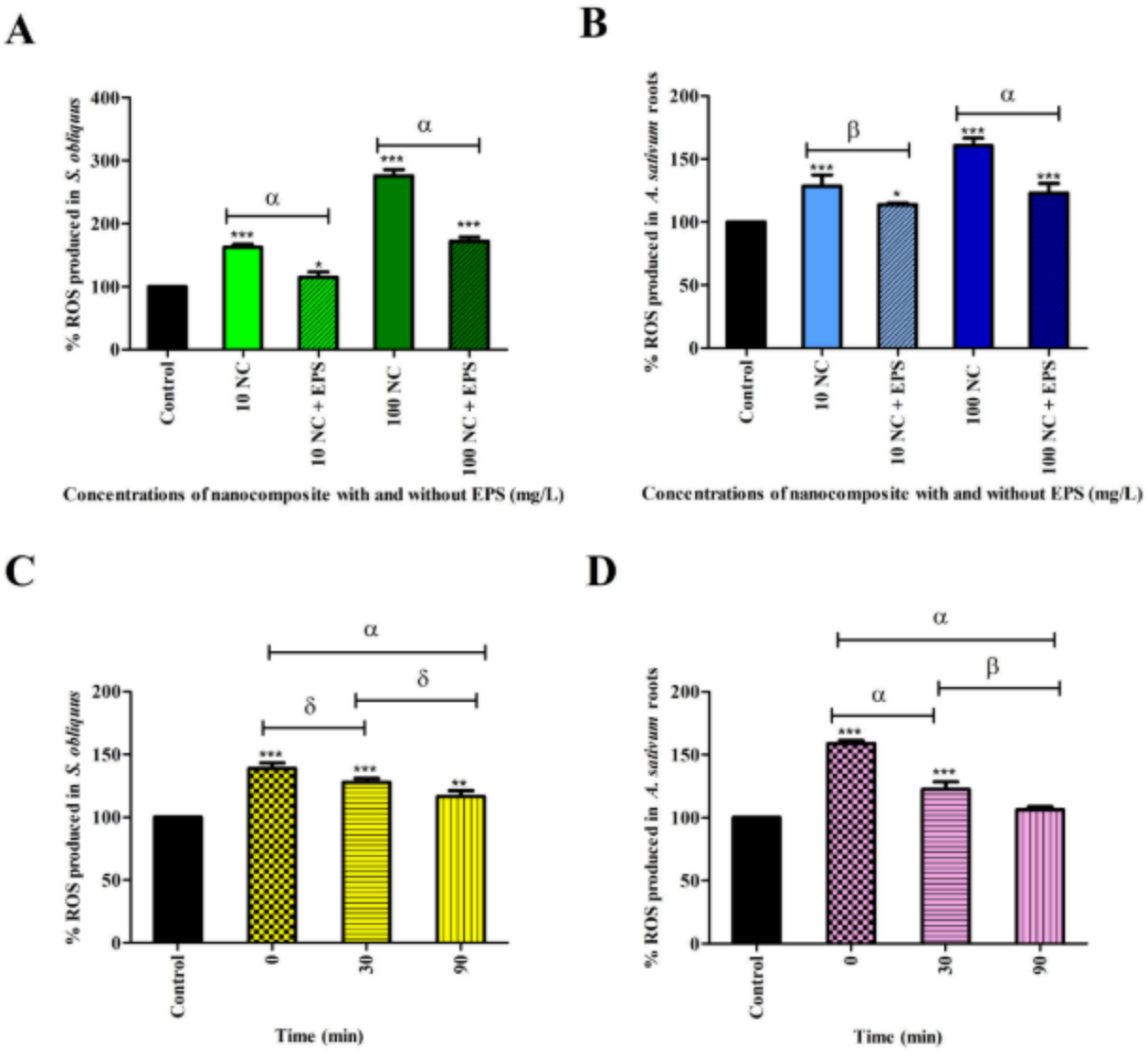


Figure 8

(A) Reactive oxygen species (ROS) production in the cells of *Scenedesmus obliquus* exposed to nano zinc oxide-zeolite nanocomposites (NC) with and without extracellular polymeric substances (EPS). (B) % ROS production in *Allium sativum* roots exposed to nano zinc oxide-zeolite NC with and without EPS. (C) % ROS production in *Scenedesmus obliquus* cells following bisphenol A (BPA) removal. (D) % ROS production in *Allium sativum* roots following BPA removal. The level of significance between the treatment vs control groups is shown by '***'-$p < 0.001$, '**'-$p < 0.01$, and '*'-$p < 0.05$, and between the treated groups is shown by 'α'- $p < 0.001$, 'β'- $p < 0.01$, and 'δ'- $p > 0.05$.

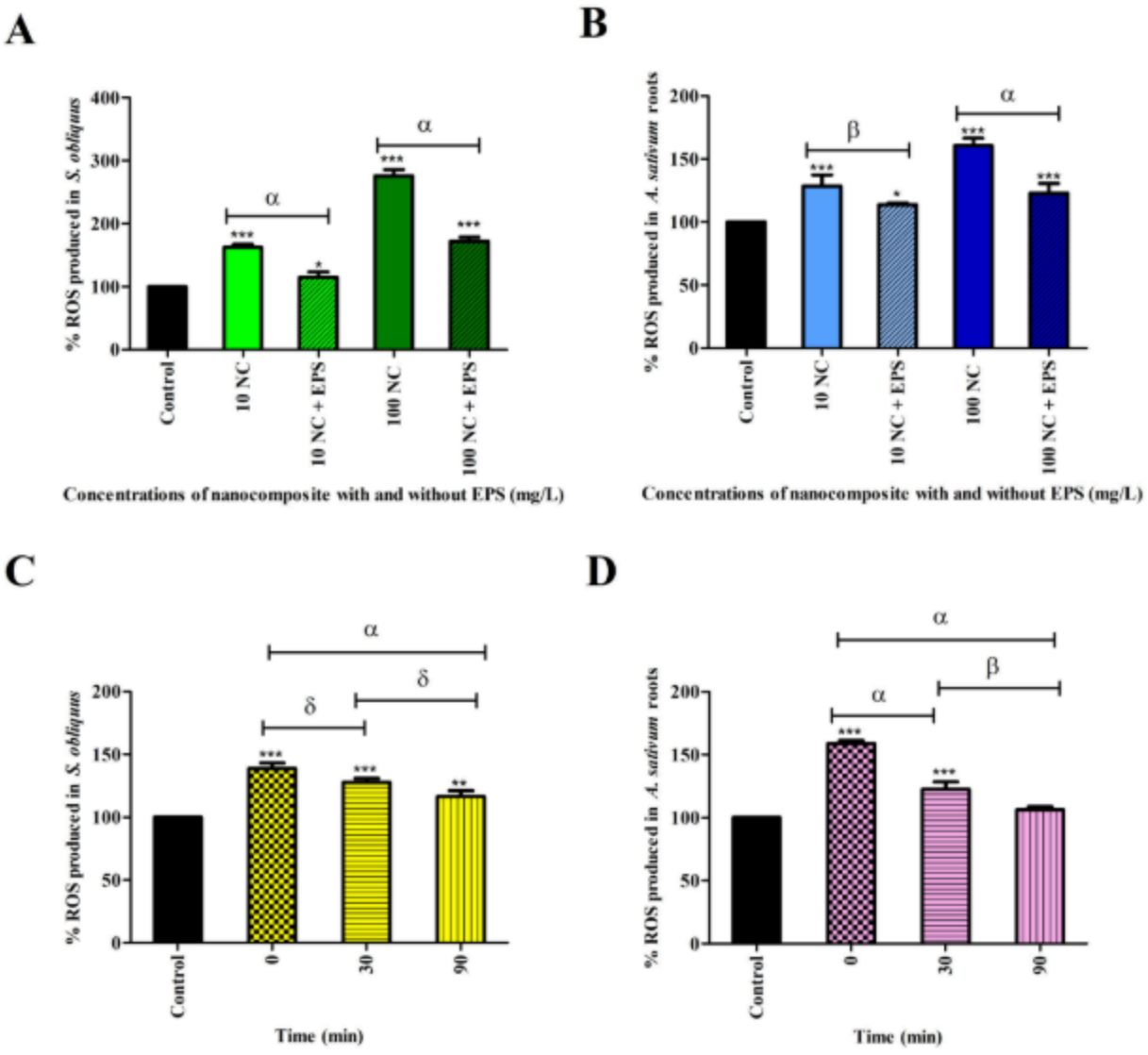


Figure 8

(A) Reactive oxygen species (ROS) production in the cells of *Scenedesmus obliquus* exposed to nano zinc oxide-zeolite nanocomposites (NC) with and without extracellular polymeric substances (EPS). (B) % ROS production in *Allium sativum* roots exposed to nano zinc oxide-zeolite NC with and without EPS. (C) % ROS production in *Scenedesmus obliquus* cells following bisphenol A (BPA) removal. (D) % ROS production in *Allium sativum* roots following BPA removal. The level of significance between the treatment vs control groups is shown by '***'-$p < 0.001$, '**'-$p < 0.01$, and '*'-$p < 0.05$, and between the treated groups is shown by 'α'- $p < 0.001$, 'β'- $p < 0.01$, and 'δ'- $p > 0.05$.

Supplementary Files

This is a list of supplementary files associated with this preprint. Click to download.

- SupplementaryFile.docx

- SupplementaryFile.docx
- SupplementaryFile.docx
- SupplementaryFile.docx
- floatimage1.jpeg
- floatimage1.jpeg
- floatimage1.jpeg
- floatimage1.jpeg